**Miltefosine increases macrophage cholesterol efflux and inhibits NLRP3-inflammasome assembly and IL-1β release.**

Iacano: Miltefosine inhibits macrophage IL-1β release

Amanda J Iacano[1], Harvey Lewis[1], Jennie E Hazen[1], Heather Andro[1], Jonathan D Smith[1,2*], and Kailash Gulshan[1*]

[1]Department of Cellular and Molecular Medicine, Cleveland Clinic, Cleveland OH 44195, USA.

[2]Department of Cardiovascular Medicine, Cleveland Clinic, Cleveland OH 44195, USA.

Total Word count: 7867

Word count of abstract: 208

Total characters with spaces: 54,176

Numbers of figures: 7

*****Correspondence to: Kailash Gulshan, Ph.D. or Jonathan D. Smith, Department of Cellular and Molecular Medicine, Cleveland Clinic, Cleveland OH , 9500 Euclid Avenue, Box NC10 Cleveland, OH 44195, Phone: 216-445-3699), Email: gulshak@ccf.org or smithj4@ccf.org.

Key Words: Cholesterol; ATP Binding Cassette Transporter A1; Autophagy; Inflammation

**Abstract:**

We tested Miltefosine, an FDA approved drug, for multiple effects in macrophages including cholesterol efflux, phospholipid trafficking, autophagy, and inflammation. Miltefosine increased ABCA1 mediated cholesterol efflux in RAW264.7 macrophages in absence of any cholesterol acceptor. Miltefosine increased lipid-raft disruption and cell surface phosphatidylserine (PS) exposure via decreased flip of PS from the cell-surface. Miltefosine treatment induced redistribution of phosphatidylinositol 4,5-bisphosphate from the plasma membrane to the actin rich regions in the cells. Miltefosine induced basal autophagy as indicated by increased p62 and LC3-II puncta formation. Free cholesterol levels were increased via degradation of lipid-droplets in Miltefosine treated cells. TLR4 signaling pathway was blunted by Miltefosine in mouse bone marrow derived macrophages, leading to ~75% reduction in pro-IL-1β mRNA levels. Miltefosine potently inhibited NLRP3 speck formation and the release of mature IL1-β. However, Miltefosine did not alter AIM2 inflammasome activity, indicating specific targeting of NLRP3 inflammasome pathway by Miltefosine. Endotoxin induced reactive oxygen species generation was significantly blunted by Miltefosine. Miltefosine pretreatment also prevented endotoxin mediated loss of mitochondrial membrane potential. Overall, Miltefosine targets multiple pathways in macrophages that are involved in atherosclerosis, inflammation, and metabolic diseases. The detailed investigation of mechanisms involved in Miltefosine's action may lead to novel therapeutic targets for treating inflammatory disease such as atherosclerosis.

**Non-standard abbreviations and acronyms:**
ABCA1, ATP-binding cassette transporter A1
AIM2, absence in melanoma 2
AMPK, AMP-activated protein kinase
apoA1, apolipoprotein A-I
ASC1, apoptosis-associated speck protein containing a CARD (Caspase activation and recruitment domain)
Gsdmd; Gasdermin D
HDL-C, high-density lipoprotein-cholesterol
IL1-β, Interleukin 1-beta
NLRP3, NOD-like receptor family pyrin domain-containing 3
NF-kB, nuclear factor kappa-light-chain-enhancer of activated B cells
PIP2, phosphatidylinositol 4,5-bisphosphate
PS, phosphatidylserine
TLR, toll like receptor

**Significance Statement:**

Atherosclerosis is driven by cholesterol accumulation and inflammation, and the arterial macrophage is a key cell type in both of these processes. The macrophage characteristics that protect against atherosclerosis include increased cholesterol efflux/reverse cholesterol transport, increased autophagy, and deceased inflammatory cytokine production and signaling. Here, we show that one single orally available compound, Miltefosine, can target multiple macrophage pathways involved in lipid homeostasis and inflammation. Miltefosine activated cholesterol efflux and autophagy while inhibited pro IL-1β gene expression and NLRP3 inflammasome assembly. In addition, Miltefosine reduced endotoxin-mediated mitochondrial reactive oxygen species and protected the mitochondrial membrane potential. The detailed investigation of mechanisms involved in Miltefosine's action may lead to novel therapeutic targets for preventing and treating atherosclerotic cardiovascular diseases.

**Introduction:**

Atherosclerosis, a sterile inflammatory disease, is the major cause of coronary artery disease (CAD). LDL cholesterol drives atherosclerosis by depositing LDL into the arterial intima, where it can be modified to induce endothelial cell activation and the recruitment of leukocytes; and, the uptake of modified LDL into macrophages leads to foam cell formation and a further amplification of inflammation (1-4). Accumulation of oxidized lipids and cholesterol crystals in plaques activate toll-like receptor (TLR) pathways and the assembly of the NLRP3 inflammasome (2, 5). The NLRP3 inflammasome is activated in aortas of advanced atherosclerosis patients as well as in other metabolic diseases such as obesity and insulin resistance (6-9). The NLRP3 inflammasome plays a key role in processing procaspase 1 resulting in subsequent caspase 1 mediated processing of pro IL-1β to generate active interleukin-1β (IL-1β). The role of IL-1β in promoting human CAD was highlighted by the recently concluded CANTOS trial, showing that anti-IL-1β therapy met the primary endpoint, a reduction in a composite of heart attack, stroke and cardiovascular death (10). The chronological activation of TLR (for production of IL-1β mRNA) and NLRP3 (for processing and release of IL-1β) in advanced atherosclerotic plaques can lead to amplification of immune responses and plaque instability.

In contrast to atherogenic pathways, the atheroprotective pathways such as autophagy and cholesterol efflux become increasingly dysfunctional in aging, advanced atherosclerotic plaques, and in animal models of atherosclerosis and diabetes (5, 11, 12). During lipophagy, lipid droplets are engulfed by autophagosomes that then fuse with lysosomes where cholesterol esters are hydrolyzed to generate free cholesterol (11, 12). Many lines of evidence have shown that inhibition of autophagy by pharmacological or genetic intervention is associated with increased atherosclerotic plaque burden (5, 11, 13). Once the free cholesterol

is generated by lipid-droplet autophagy it can be transported back to liver for excretion via reverse cholesterol transport (RCT) (14-18). The first step in RCT involves ABCA1-mediated cholesterol and phospholipid efflux to generate nascent HDL; however ABCA1 expression can also disrupt lipid-rafts and dampen TLR recruitment to cell membrane (19). Thus, the simultaneous induction of athero-protective pathways, such as cholesterol efflux and autophagy, along with dampening of atherogenic pathways such as TLR signaling and NLRP3 inflammasome assembly, may serve as a potent therapeutic treatment for CAD patients. Here, we report that Miltefosine, an FDA approved drug for treating visceral and cutaneous leishmaniasis, promoted cholesterol efflux, disrupted lipid-rafts and TLR4 signaling, increased cell-surface phosphatidylserine (PS) exposure, induced phosphatidylinositol 4,5-bisphosphate (PIP2) trafficking from plasma membrane (PM) to the cell interior, induced basal autophagy, reduced lipopolysaccharide (LPS) induced mitochondrial reactive oxygen species (ROS) generation, and blunted NLRP3 inflammasome assembly and IL-1β release.

**Results:**

**Miltefosine induced ABCA1 mediated cholesterol efflux from cells**

Previous study have shown that Miltefosine and other alkylphospholipids induced cholesterol efflux from the HepG2 cells(20). We tested effect of Miltefosine treatment on ABCA1 mediated cholesterol efflux in RAW264.7 macrophages. Control and ABCA1 expressing cells were incubated with different doses of Miltefosine for 4h and cholesterol efflux to serum-free media in the absence of apoA1, the usual acceptor, was determined. As shown in ***Fig. 1A***, Miltefosine treatment of control cells without ABCA1 expression led to a dose dependent moderate, but significant, increase in cholesterol efflux to media, with 7.5 μM showing ~1 % increase ($n=4$, $p<0.001$) and 10 μM showing ~2.8 % increase vs. control cells ($n=4$, $p<0.0001$).

The ABCA1-expressing cells showed more robust cholesterol efflux to acceptor-free media in presence of Miltefosine with 7.5 μM showing ~5.28 % increase (n=4, $p<0.01$) and 10 μM showing ~10.9 % increase vs control cells, (n=4, $p<0.0001$). Western blot analysis of total and cell-surface ABCA1 showed no major differences in control vs. Miltefosine treated cells (***Fig. 1B***), indicating that Miltefosine induced increase in cholesterol efflux was not due to increased ABCA1 levels. Further studies use 7.5 μM of less of Miltefosine, as these doses do not lead to cell death based on LDH release assay (***Fig. S1A, B***). We observed the Miltefosine induction of cholesterol efflux in two additional cell lines, HEK293 and BHK. In both cases, addition of Miltefosine induced basal cholesterol efflux, and markedly induced ABCA1-mediated cholesterol efflux to the acceptor-free media (***Fig. 1C, S1C***). To test if the lipid floppase activity (outward translocation across the plasma membrane) of ABCA1 is required for increased cholesterol efflux in Miltefosine treated cells, we used HEK293 cells stably expressing WT-ABCA1 isoform or a Tangier disease double mutant W590S-C1477R-ABCA1 isoform. The WT ABCA1 can flop phosphatidylserine (PS) and phosphatidylinositol 4,5-bisphopshate (PIP2) across plasma membrane (21). The W590S mutation in ABCA1 decreases PS flop (22) while C1477R decreases PIP2 flop (21). The HEK293 cells expressing WT and double mutant isoform of ABCA1 were loaded with radiolabeled cholesterol and cholesterol efflux to media was determined in presence and absence of Miltefosine. The W590S-C1477R double mutant isoform of ABCA1, with protein expression levels slightly higher than WT ABCA1 (***Fig. S1D***), showed significantly lower cholesterol efflux to acceptor-free media compared to WT-ABCA1 (***Fig. 1D***), indicating that lipid floppase activity of ABCA1 promotes the Miltefosine induced cholesterol efflux to media. It has previously been shown that ABCA1 expression promotes membrane blebbing and the release of microparticles (23). We determined the effect of Miltefosine on generation of microparticles by cells. The media from RAW264.7 macrophages

incubated ± Miltefosine for 4h was collected and analyzed by a small particle tracking analyzer. The media from the cells treated with Miltefosine had significantly 2-fold more microparticles compared to control cells (P<0.001, ***Fig. S2***). These data indicated that Miltefosine mediated remodeling of the plasma membrane promotes release of microparticles leading to cellular cholesterol efflux to the media, which was even greater in the presence of ABCA1 expression.

**Miltefosine disrupts lipid rafts and increased PS exposure by inhibiting PS flip**

Lipid rafts are comprised mainly of PC, cholesterol and sphingomyelin (24), and play a role in AKT and TLR signaling pathways. Disruption of lipid-rafts by ABCA1 is proposed to provide a free cholesterol pool for efflux and hamper TLR signaling via reduced recruitment of TLR2/4 to lipid-rafts (19, 25, 26). Previous studies have also shown that Miltefosine uses lipid-rafts as entry portals to cells (27) and can act as a lipid-raft disrupting agent to inhibit human mast cell activation (28). We determined the status of lipid-rafts in Miltefosine treated RAW264.7 macrophages by staining for the ganglioside GM1 using Alexa647-labeled cholera toxin B, followed by either fluorescent microscopy or flow cytometry. As shown in ***Fig. 2A*** cells treated with 7.5 μM Miltefosine for 16h displayed less GM1 vs. control cells. Flow cytometry quantification showed ~ 26% GM1 decrease in Miltefosine treated vs. control cells (n=3, p<0.004 by t-test, ***Fig. 2B***). We have previously shown that membrane remodeling by sphingomyelin depletion resulted in lipid raft disruption, increased cell-surface PS, and promoted cholesterol extraction from cells (29). A flow-cytometry based Annexin Cy5 binding assay was used to investigate if Miltefosine increased PS exposure at the cell-surface. Cells expressing ABCA1 were used as positive control, as PS cell-surface exposure is increased by ABCA1's PS flop activity (21, 22). As shown in ***Fig. 2C***, Miltefosine treated cells showed ~24% increase in cell surface PS vs. untreated cells (n=4, p<0.005). As expected, the cells expressing ABCA1 also showed increased PS exposure (~23% increase vs control cells, n=4,

p<0.05). Cell surface PS was further increased by Miltefosine treatment in ABCA1 expressing cells (~39% increase vs. control cells, n=4, p<0.0005). These data indicates that Miltefosine increased cell-surface PS exposure independent of ABCA1 PS floppase activity. The increased levels of cell surface PS may be due to the decreased rate of PS flipping (inward translocation). To qualitatively observe the PS flipping across plasma membrane (PM), RAW264.7 cells ± 7.5uM Miltefosine treatment for 16h, were incubated with exogenously added NBD-PS at final concentration of 25 μM. In control cells, the majority of exogenous NBD-PS moved to intracellular compartments over a 15 min incubation period at 37ºC, while Miltefosine treated cells displayed more NBD-PS at the PM and less inside the cells (***Fig. 2D***). To quantitatively measure flipping of NBD-PS, we used a previously described flow-cytometry based method using a membrane-impermeable NBD quenching reagent sodium dithionite (29). RAW cells treated with ± 7.5uM Miltefosine for 16h were incubated with NBD-PS for 15 min at 37°C, followed by addition of sodium dithionite to selected aliquots and flow cytometry analysis. The amount of NBD-PS flipped into the cells was calculated by measuring the % of NBD fluorescence resistant to quenching by sodium dithionite. As shown in ***Fig. 2E***, Miltefosine treated cells flipped significantly lower amounts of NBD-PS vs. control cells, ~44% vs. ~70% respectively (n=4, p<0.0002). These data indicate that Miltefosine inhibited PS flip from the cell surface, resulting in increased PS exposure at the cell surface.

**PIP2 is redistributed from plasma membrane upon Miltefosine treatment**

Similar to PS, phosphatidylinositol 4, 5-bisphosphate (PIP2) is also sequestered in the inner leaflet of the plasma membrane. To determine the effect of Miltefosine on PIP2 trafficking and localization, RAW264.7 cells were stably transfected with a PIP2 reporter plasmid containing 2 copies of the pleckstrin homology domain from phospholipase Cδ fused to GFP (2X-PH-PLC-eGFP). These cells were treated with ± 7.5 μM Miltefosine for 16h and PIP2 reporter

localization was determined by fluorescent microscopy. As shown in ***Fig. 3A***, control cells showed uniform localization of the PIP2 reporter at the plasma membrane while the cells treated with Miltefosine showed an additional localization of the reporter in a specific actin rich region of the cytoplasm in both fixed and live cells (***Fig. 3B, C***).

**Miltefosine induced basal and lipid-droplet autophagy**

Autophagy plays a protective role against atherosclerosis (12) and becomes increasingly impaired in advanced human plaques (11). Autophagy is required for hydrolyzing macrophage cholesterol ester stored in lipid droplets to generate free cholesterol that can be effluxed from cells (12). As Miltefosine increases cholesterol efflux, we tested if Miltefosine induced autophagy. We observed that the RAW264.7 macrophages treated with 7.5 μM Miltefosine for 16h showed multiple p62 puncta in cytoplasm, while control cells had evenly distributed weak cytoplasmic signal with almost no p62 puncta signal (***Fig. 4A,*** upper panel). Miltefosine treatment also increased LC3 puncta formation in macrophages transfected with LC3-GFP plasmid (***Fig. 4A*** lower panel). Next, we evaluated whether the LC3 puncta formation was due to increased autophagic initiation or due to decreased autophagic flux. Decreased or blocked autophagy flux can also lead to accumulation of autophagic markers. If western blot analysis shows increased LC3-II after chloroquine (an autophagy flux inhibitor) treatment, then autophagic flux is occurring. We found that the LC3-II protein levels were increased by 3.5-fold in Miltefosine treatment alone vs. control cells (***Fig. 4B, 4C***), while there was an additional 1.8 fold increase in LC3-II protein levels with Miltefosine + chloroquine treatment compared to cells treated with Miltefosine alone. These data indicate that Miltefosine increased autophagic flux. Next, we tested the effect of Miltefosine on generation of free cholesterol from cholesterol ester rich lipid droplets. RAW264.7 macrophages were loaded with 100 μg/ml acetylated LDL (AcLDL) for 24h followed by a 4h chase with an acyl-co A cholesterol O-acyltransferase

(ACAT) inhibitor (ACATi) to prevent cholesterol re-esterification ± 7.5 µM Miltefosine. The total and free cholesterol levels were determined by enzymatic assay described previously (30). As expected, the AcLDL loaded cells had a higher ratio of cholesterol ester to free cholesterol (***Fig. 4D***). The cells chased with ACATi had reduced CE:FC ratio ($P<0.05$ vs. control), while the Miltefosine + ACATi treated cells showed further lowering of CE:FC ratio ($p<0.01$ vs. control). We also tested the effect of Miltefosine on lipid-droplets by loading RAW264.7 cells with 100µg/ml AcLDL for 24h, followed by a 4 h chase with ± Miltefosine and staining with Nile-red dye. Cells treated with Miltefosine showed reduced Nile-red staining as compared to control cells (***Fig. S3***). To quantify the lipid-droplets, AcLDL loaded cells were chased for 4h with ACATi ± Miltefosine and subjected to flow-cytometry analysis. A shown in ***Fig. 4E***, the cells chased with ACATi showed decreased lipid droplets that were further decreased by Miltefosine ($n=4$, $p<0.0001$). These data indicate that Miltefosine induced lipid-droplet autophagy as ACATi prevents new CE formation. The levels of phosphorylated AMPK were higher in Miltefosine vs. control cells with ~ 1.5 fold increase in p-AMPK::AMPK ratio (***Fig S4***).

**Miltefosine decreased LPS mediated induction in IL-1β levels**

We demonstrated in ***Fig 2A*** that Miltefosine reduces lipid-rafts, which play an essential role in TLR2/4 signaling pathway and atherosclerosis progression (19, 25, 31-33). We tested if LPS mediated induction of pro IL-1β mRNA was affected by Miltefosine. Bone-marrow derived macrophages (BMDMs) ± Miltefosine pretreatment were incubated with 1 µg/ml LPS for 4h, followed by qRT-PCR using IL-1β specific primers and control Actb (β-actin) primers. The LPS induction of IL-1β mRNA was markedly reduced in Miltefosine treated cells (~4.5 fold decrease, $n=3$, $p<0.034$) (***Fig. 5A***). Western blot analysis of pro IL1-β protein in LPS control vs. LPS+Miltefosine treated cells revealed a similar effect of Miltefosine with a ~55% decrease

(***Fig. 5B)***. Taken together, these data indicate that Miltefosine disrupted lipid-rafts and decreased the LPS mediated induction of IL-1β mRNA and protein levels in macrophages.

**Miltefosine inhibited NLRP3 inflammasome assembly and IL-1β release**

Cholesterol crystals, as well as other treatments including extracellular ATP, lead to NLRP3 inflammasome assembly which processes pro IL-1β to its mature form for secretion from cells (2, 34). Control and BMDMs pretreated with 5 μM Miltefosine for 16h, were primed with LPS for 4h and incubated with ATP for 20 min, followed by probing with anti-ASC antibody for visualization of NLRP3 inflammasome assembly. BMDMs treated with LPS and ATP formed ASC specks in 41% cells (n=308 cells analyzed) while in BMDMs pretreated with Miltefosine only 12% of cells showed ASC specks (523 cells analyzed, $p<0.0001$ by two-tailed Fisher's exact test) (***Figs.6A, S5, S6***). Miltefosine treatment led to ~75% decrease in release of mature IL-1β to media as compared to control macrophages (n=3, $p<0.0039$) (***Fig. 6B***). To decipher the mechanism by which Miltefosine inhibited NLRP3 inflammasome assembly, we determined the mRNA and protein levels of the constituents of the NLRP3 inflammasome and one substrate Gasdermin D (Gsdmd) in BMDMs with or without LPS priming. Miltefosine with LPS actually slightly increased the mRNA levels, beyond the effects of LPS alone, for NLRP3, procaspase 1 and Gasdermin D (***Fig. 6C***). In agreement with earlier published studies (35), western blot analysis showed robust induction in protein levels of NLRP3 upon LPS treatment, which was not reduced by Miltefosine treatment (***Fig. S7)***. Miltefosine did not appreciably alter the protein levels of ASC or procaspase 1 ***(Fig. S7)***. The release of mature IL-1β from cells is regulated by Gasdermin D mediated pore formation on the plasma membrane (36, 37). We tested and found no alteration in Gasdermin D protein levels by Miltefosine treatment (***Fig. S7***). To test if Miltefosine specifically inhibited NLRP3 inflammasome assembly and IL-1β release, we determined the effects of Miltefosine on the AIM2 inflammasome. The control and

Miltefosine treated macrophages were primed with LPS (1mg/ml) for 4hrs followed by lipofectamine mediated transfection of poly (dA:dT) for 3h. As shown in ***Fig. 6D***, there was no difference in levels of AIM2 induced IL-1β released from cells ± Miltefosine treatment (n=3, n.s.); thus, Miltefosine did not alter AIM2 inflammasome activity. Previous studies have shown that the deficiency of ABCA1/ABCG1 increases inflammation in macrophages while ABCA1 mediated cholesterol efflux in dendritic cells dampens inflammasome assembly (38, 39). Though, we used unloaded BMDMs for these studies, there is a possibility that Miltefosine inhibits NLRP3 inflammasome assembly via cholesterol depletion. To directly test the role of cholesterol depletion on NLRP3 inflammasome assembly, we treated BMDMs with 5μM Miltefosine for 16h or with 1mM cyclodextrin for 45 minutes at 37$^{o}$C, followed by LPS/ATP incubation. Although cholesterol levels in BMDMs treated with cyclodextrin were significantly lower compared to Miltefosine treated cells (n=3, $p<0.01$, ***Fig. 6E***), Miltefosine was much more effective than cyclodextrin in inhibiting inflammasome activity as assayed by IL-1β release (***Fig. 6F)*** and ASC speck formation (***Fig. S5, S8***). Thus, NLRP3 inflammasome inhibition by Miltefosine cannot be attributed solely to cholesterol depletion.

**Miltefosine reduced endotoxin mediated mitochondrial ROS production and loss of mitochondrial membrane potential.**

Since Miltefosine treatment did not reduce the expression levels of NLRP3 inflammasome pathway components such as NLRP3, ASC, Caspase 1 or Gasdermin D, we tested if Miltefosine affected mitochondrial reactive oxygen species (ROS) generation. Mitochondrial ROS drives NLRP3 inflammasome assembly (40) and mitochondrial cardiolipin provides a docking site for NLRP3 protein binding and inflammasome assembly (41). As shown in ***Fig. 7A***, LPS treatment induced ROS production in control BMDMs as evident by increased staining with MitoSox Red while the Miltefosine pretreated cells showed decreased MitoSox

staining upon LPS treatment. To quantify the MitoSox signal, we performed flow-cytometry and found that Miltefosine treated cells showed a significant 43% reduction in LPS-induced MitoSox staining (***Fig. 7B).*** Next, we tested the effect of Miltefosine on the mitochondrial membrane potential. Control and Miltefosine pretreated BMDMs were incubated with ± LPS for 1h and stained with tetramethylrhodamine (TMRM) for 30 min at 37ºC, followed by fluorescent microscopy of live cells. The cells treated with LPS showed marked reduction in TMRM staining while cells pretreated with Miltefosine partially rescued the mitochondrial membrane potential (***Fig. S9***). To quantify the TMRM signal, we performed flow-cytometry and found that LPS treated cells showed a significant 41% reduction in TMRM staining signal while cells pretreated with Miltefosine showed only a 24 % reduction (***Fig. 7C)***. Given that Miltefosine induced autophagy in macrophages, we tested role of Miltefosine in removing damaged mitochondria from via mitophagy. Live RAW264.7 macrophages were loaded with 500 nM mitophagy indicator dye for 30 min at 37ºC, followed by treatment with ± Miltefosine for 4h. The control cells showed weak fluorescence while cells treated with Miltefosine showed bright fluorescence (***Fig. S10)***. To determine if the mitochondria were indeed fused with lysosomes, a lysosomal stain was used. As compared to control cells, the cells treated with Miltefosine showed markedly increased co-localization of the mitophagy and lysosome dyes (***Fig. 7D***). Thus, Miltefosine may inhibit inflammasome assembly by decreasing mitochondria ROS, preventing LPS mediated damage to mitochondria, and by removing damaged mitochondria through mitophagy.

## Discussion

Miltefosine is on the World Health Organization list of essential medicines and is FDA approved for treating cutaneous and visceral leishmaniasis. The structure of Miltefosine is similar to lyso-PC and it is known to integrate in the cell membrane and redistribute in

intracellular membranes of ER, Golgi and mitochondria (42). It is widely believed that most of the downstream effects of Miltefosine are dependent on cell-type, with a range of activities such as induction of apoptosis in cancer cells, effects on cholesterol homeostasis, and inhibition of Mast cell activation (28, 42-44). However, the mechanism of action of Miltefosine, whether regarding killing of parasites or cancer cells is not fully understood.

We found that Miltefosine has multiple activities in macrophages; induction of cholesterol efflux from cells via the release of microparticles, lipid-raft disruption, inhibition of PS flip from the outer to the inner leaflet of the plasma membrane, redistribution of plasma membrane PIP2 to cytoplasmic actin-rich regions, induction of basal autophagy, increased lipid droplet turnover, and inhibition of NLRP3 inflammasome assembly/IL-1β release. Cholesterol efflux in the absence of an exogenous acceptor has been shown to be due to microparticle generation that is increased by ABCA1 expression (45), and Miltefosine effects on the plasma membrane may alter membrane fluidity to increase microparticle generation. The Miltefosine increase in ABCA1-mediated cholesterol efflux requires functional lipid floppase activity as the ABCA1 mutant isoform defective in PS and PIP2 floppase activity showed lower cholesterol efflux to media in presence of Miltefosine. Thus, the Miltefosine mediated increase in cell surface PS and the disruption of lipid-rafts may lead to a redistribution of lipids to promote microparticle release.

Miltefosine's effect on PIP2 localization may affect many cellular processes. In addition to its well defined role as a precursor of the diacylglycerol and inositol triphosphate following its hydrolysis by phospholipase C, intact PIP2 plays an important role in membrane ruffling, microvilli formation, endocytosis, phagocytosis and the attachment of membrane to cytoskeleton (46). Miltefosine was initially identified as anti-cancer compound and is known to inhibit AKT signaling pathway (42). Alkylphosphocholines such as Miltefosine are proposed to

prevent plasma membrane recruitment of the PH domain of AKT by disrupting plasma membrane microdomains (47). PIP2 serves as substrate for generation of PIP3 at cell membrane and PIP3 can activate AKT signaling. We speculate that Miltefosine effects on PIP2 localization could also play a role in AKT inhibition as reduced localization of PIP2 at plasma membrane by Miltefosine can deplete PIP3 pool at plasma membrane and reduce AKT signaling.

Autophagy plays a protective role in atherosclerosis and it is impaired in advanced human plaques (11-13). Autophagy is controlled by multiple pathways responding to stimuli such as the status of cellular energy (AMP-dependent protein kinase, AMPK) or amino acid availability (target of rapamycin, TOR). Miltefosine induced basal autophagy in macrophages as evident by increased cytoplasmic p62 and LC3-GFP puncta. We showed that Miltefosine treatment increased the turnover of cholesterol esters in cholesterol loaded cells, supporting the notion that Miltefosine increased degradation of lipid-droplets via lipophagy. The increased phosphorylation of AMPK due to Miltefosine may lead to induced basal autophagy that we observed in Miltefosine treated cells. AMPK is a key regulator of lipid and energy metabolism and decreased AMPK activity due to aging or inflammation may promote metabolic disorders such as cardiovascular disease and diabetes (48).

Lipid-rafts play an essential role in recruiting TLRs to plasma membrane to initiate a signaling cascade that allows cytoplasmic NF-kB to shuttle inside the nucleus and upregulate inflammatory genes such as pro IL-1β mRNA and NLRP3. Miltefosine markedly reduced the LPS mediated induction of pro IL-1β mRNA. However, NLRP3 mRNA levels after LPS induction were similar in Miltefosine treated and control cells. Since both IL-1β and NLRP3 mRNAs are induced by NF-kB, the different response to NF-kB may in part be explained by their different degrees of induction, as NLRP3 mRNA was modestly increased (3-fold)

compared to the robust (30,000- fold) induction of pro IL-1β mRNA. Thus, the detailed mechanism for the TLR-mediated induction of these two genes may differ.

The components of the inflammasome complex, NLRP3, ASC, and Caspase1 are significantly increased in atherosclerotic plaques compared to healthy arteries. Blocking of NLRP3 by the small molecule MCC9550 reduces atherosclerosis in mouse and infarct size in pigs (49, 50); and, a recent trial showed reduced cardiovascular events in subjects treated with an anti IL-1β monoclonal antibody (10). The protein levels of NLRP3 are not only controlled transcriptionally, but also by a non-transcriptional pathway involving TLR4 and Myd88 via NLRP3 deubiquitination (35). Although Miltefosine inhibited NLRP3 inflammasome assembly, surprisingly, the levels of NLRP3 inflammasome components (ASC, NLRP3, and pro Caspase 1) in resting as well as in LPS induced macrophages were unaltered in control vs. Miltefosine treated cells. Mature IL-1β is released via cleaved Gasdermin D pores (51), but Miltefosine treatment did not alter the levels of full length Gasdermin D, thus ruling out decreased Gasdermin D as a mechanism for Miltefosine. The intriguing question raised by these data is that if all inflammasome components are present and more or less equally expressed in control vs. Miltefosine treated macrophages, why is the NLRP3 inflammasome not assembled in Miltefosine treated cells? Recently it was shown that NLRP3 is localized to the trans golgi network via binding to PI4P prior to inflammasome assembly (52). Miltefosine may work at this or other steps to block inflammasome assembly. Alternatively, Miltefosine changes in the plasma membrane may diminish K+ efflux required for inflammasome assembly. Mitochondria also play an essential role in assembly of the NLRP3 inflammasome (40, 53), and Miltefosine treated cells showed reduced levels of ROS upon LPS treatment, which may also effect NLRP3 inflammasome assembly. Here we have shown that Miltefosine has many activities in macrophages that collectively should lead to a reduction in lipid storage and inflammation.

Thus, Miltefosine may be an attractive molecule for future preclinical studies in atherosclerosis, inflammatory diseases, and metabolic disorders, such as diabetes, non-alcoholic fatty liver disease, and obesity (54-56).

## Material and Methods

A detailed description of the materials and methods used in this study is provided in *SI Materials and Methods*. Basic methods are summarized below.

**Cell culture and reagents:** Cells were grown in Dulbecco's Modified Eagle Medium (DMEM) with 10% fetal calf serum, 100 µg/mL penicillin, 100 µg/mL streptomycin. Mifepristone ABCA1-inducible BHK cells, as previously described were obtained from Chongren Tang, University of Washington (57). ABCA1-GFP and the mutant isoform stably transfected HEK cells were previously described (58). Other materials are described in *SI Materials and Methods*.

**Isolation of Bone marrow derived macrophages:** Mice were maintained on chow diet and femurs were collected to isolate and culture bone marrow macrophages using 20% L-cell conditioned media. Other details are described in *SI Materials and Methods*.

**Isolation of total RNA from BMDM cell pellets and RT-PCR analysis:** Total RNA was isolated from cell pellets using the RNeasy Mini Kit (Qiagen, Valencia, CA), following the manufacturer's protocol. On-column digestion with RNase-free DNase (Qiagen, Valencia, CA) was performed to remove genomic DNA. qRT-pCR assays were performed using TaqMan reagents from ThermoFisher following the manufacturer's protocol. Other materials and details are described in *SI Materials and Methods*.

**Cholesterol efflux assay**: Cholesterol efflux assays were performed in HEK293-ABCA1-GFP cells, BHK cells, or RAW264.7 murine macrophages as described earlier (21). Other details are described in *SI Materials and Methods*.

**Lipid-Raft quantification**: The lipid-raft were visualized using Alexa647-labeled cholera toxin B subunit and fluorescent microscopy, with quantification by flow-cytometry assay as described before (29). Other details are described in *SI Materials and Methods*.

**Mitochondrial ROS production and membrane potential measurement:** Mitochondrial ROS levels were determined in control or Miltefosine treated BMDMs that were primed with 1ug/ml LPS for 4h, followed by staining with MitoSOX™ Red Mitochondrial Superoxide Indicator (ThermoFisher) using manufacturer's protocol. Cells were either visualized by fluorescent microscopy or subjected to flow-cytometry analysis. Mitochondrial membrane potential measurements were determined in control or Miltefosine treated BMDMs that were primed with 1ug/ml LPS for 4h, followed by staining with Image-iT™ TMRM Reagent (ThermoFisher) using manufacturer's protocol. Cells were visualized by fluorescent microscopy or subjected to flow-cytometry analysis.

**Total/FC measurements:** RAW264.7 cells were loaded with 100 µg/ml AcLDL for 16 h at 37 °C with or without 2 µg/ml ACATi (Sandoz 53-035, Sigma) treatment for 2h. The total cholesterol and free cholesterol levels were determined by using enzymatic assay as described earlier (30).

**Cell-surface PS and NBD-PS translocation:** The flow cytometry based assays to determine cell-surface PS and translocation of NBD-PS were described earlier (29). Other details are described in *SI Materials and Methods*.

**Western blotting:** RAW264.7 cells or BMDMs were grown treated as indicated. Cells were lysed in NP40 lysis or MPER lysis buffer. After discarding the nuclear pellet, the protein concentration was determined using the BCA protein assay (Pierce). 10-50 µg of cell protein samples were resolved on SDS gel, followed by probing with primary and secondary

horseradish peroxidase-conjugated antibodies. Total and cell-surface ABCA1 levels were determined as described earlier (29). Other details are described in *SI Materials and Methods*.

**Cellular immunofluorescence assays:** RAW264.7 cells or BMDMs were grown in 4-chamber slides in indicated growth media. Cells were washed with 1xPBS, fixed with paraformaldehyde, and then incubated with permeabilization solution (1xPBS/0.2% Triton X-100) for 10 min at RT. Cells were washed with 1xPBS three times and blocked with normal goat serum (1xPBS/1%BSA/5% normal goat serum) at 37ºC for 30 min. The cells were probed with p62 antibody and Alexa 647 labeled secondary antibody. For LC3 staining, RAW264.7 cells were transfected with LC3-GFP (Addgene) using lipofectamine LTX according to manufacturer protocol (Life Technologies). Cells were treated with or without 7.5 μM Miltefosine for 16 h. For ASC staining, BMDM from WT C57BL6 or C57BL6 apoE$^{-/-}$ KO mice were treated ± 5 μM Miltefosine for 16 h or ± 1mM cyclodextrin for 2h. Cells were washed with 1xPBS and fixed with 100% ethanol, followed by staining with anti-ASC antibody and Alexa 568 labeled secondary antibody. All images were captured using an Olympus IX51 inverted epifluorescent microscope, Olympus LUCPlanFl ×40/0.6 lens, with a Q-Image EXi aqua camera and Olympus cellSens Dimension version 1.7 software. Post-imaging processing was performed in Adobe Photoshop CS2.

**PIP2 cellular reporter assay**: RAW264.7 macrophage cell lines stably transfected with 2PH-PLCδ-GFP plasmid was described earlier (21). Live or fixed cells were visualized by epifluorescent microscopy.

**Statistical analyses:** Data are shown as mean ± SD. Comparisons of 2 groups were performed by a 2-tailed t test, and comparisons of 3 or more groups were performed by ANOVA with Bonferroni posttest. All statistics were performed using Prism software (GraphPad).

## Author Contributions

K.G. conceived, designed, and directed research. K.G. A.J.I., H.L., and J.H. performed research. A.J.I, H.L., J.H., H.A., J.D.S., and K.G. analyzed data. A.J.I, J.D.S, and K.G. drafted the manuscript. All authors critically reviewed the manuscript.

## Acknowledgments

This research was supported by American Heart Association scientist development grant SDG25710128 to K.G and NIH grants R01 HL128268 and R01 HL130085 to J.D.S.

## Disclosures

A patent application related to this work has been filed by the Cleveland Clinic that lists K.G. and J.D.S. as inventors.

## References


1. Moore KJ & Tabas I (2011) Macrophages in the pathogenesis of atherosclerosis. *Cell* 145(3):341-355.
2. Duewell P, *et al.* (2010) NLRP3 inflammasomes are required for atherogenesis and activated by cholesterol crystals. *Nature* 464(7293):1357-1361.
3. Libby P, Ridker PM, & Maseri A (2002) Inflammation and atherosclerosis. *Circulation* 105(9):1135-1143.
4. Tall AR & Yvan-Charvet L (2015) Cholesterol, inflammation and innate immunity. *Nat Rev Immunol* 15(2):104-116.
5. Razani B, *et al.* (2012) Autophagy links inflammasomes to atherosclerotic progression. *Cell metabolism* 15(4):534-544.
6. Hansson GK & Klareskog L (2011) Pulling down the plug on atherosclerosis: cooling down the inflammasome. *Nature medicine* 17(7):790-791.
7. Zheng F, Xing S, Gong Z, & Xing Q (2013) NLRP3 inflammasomes show high expression in aorta of patients with atherosclerosis. *Heart Lung Circ* 22(9):746-750.
8. Vandanmagsar B, *et al.* (2011) The NLRP3 inflammasome instigates obesity-induced inflammation and insulin resistance. *Nature medicine* 17(2):179-188.
9. Stienstra R, *et al.* (2011) Inflammasome is a central player in the induction of obesity and insulin resistance. *Proceedings of the National Academy of Sciences of the United States of America* 108(37):15324-15329.
10. Ridker PM, *et al.* (2017) Antiinflammatory Therapy with Canakinumab for Atherosclerotic Disease. *The New England journal of medicine* 377(12):1119-1131.
11. Liao X, *et al.* (2012) Macrophage autophagy plays a protective role in advanced atherosclerosis. *Cell metabolism* 15(4):545-553.
12. Ouimet M, *et al.* (2011) Autophagy regulates cholesterol efflux from macrophage foam cells via lysosomal acid lipase. *Cell metabolism* 13(6):655-667.
13. Sergin I & Razani B (2014) Self-eating in the plaque: what macrophage autophagy reveals about atherosclerosis. *Trends in endocrinology and metabolism: TEM* 25(5):225-234.
14. Khera AV, *et al.* (2011) Cholesterol efflux capacity, high-density lipoprotein function, and atherosclerosis. *The New England journal of medicine* 364(2):127-135.
15. Wang X, *et al.* (2007) Macrophage ABCA1 and ABCG1, but not SR-BI, promote macrophage reverse cholesterol transport in vivo. *The Journal of clinical investigation* 117(8):2216-2224.
16. Yvan-Charvet L, Wang N, & Tall AR (2010) Role of HDL, ABCA1, and ABCG1 transporters in cholesterol efflux and immune responses. *Arteriosclerosis, thrombosis, and vascular biology* 30(2):139-143.
17. Oram JF (2002) ABCA1 as a New Therapeutic Target for Treating Cardiovascular Disease. *Drug news & perspectives* 15(1):24-28.
18. Oram JF (2003) HDL apolipoproteins and ABCA1: partners in the removal of excess cellular cholesterol. *Arteriosclerosis, thrombosis, and vascular biology* 23(5):720-727.
19. Zhu X, *et al.* (2010) Macrophage ABCA1 reduces MyD88-dependent Toll-like receptor trafficking to lipid rafts by reduction of lipid raft cholesterol. *Journal of lipid research* 51(11):3196-3206.

20. Rios-Marco P, Jimenez-Lopez JM, Marco C, Segovia JL, & Carrasco MP (2011) Antitumoral alkylphospholipids induce cholesterol efflux from the plasma membrane in HepG2 cells. *J Pharmacol Exp Ther* 336(3):866-873.
21. Gulshan K, *et al.* (2016) PI(4,5)P2 Is Translocated by ABCA1 to the Cell Surface Where It Mediates Apolipoprotein A1 Binding and Nascent HDL Assembly. *Circulation research* 119(7):827-838.
22. Alder-Baerens N, *et al.* (2005) Headgroup-specific exposure of phospholipids in ABCA1-expressing cells. *The Journal of biological chemistry* 280(28):26321-26329.
23. Duong PT, *et al.* (2006) Characterization of nascent HDL particles and microparticles formed by ABCA1-mediated efflux of cellular lipids to apoA-I. *Journal of lipid research* 47(4):832-843.
24. Simons K & Toomre D (2000) Lipid rafts and signal transduction. *Nature reviews. Molecular cell biology* 1(1):31-39.
25. Yvan-Charvet L, *et al.* (2008) Increased inflammatory gene expression in ABC transporter-deficient macrophages: free cholesterol accumulation, increased signaling via toll-like receptors, and neutrophil infiltration of atherosclerotic lesions. *Circulation* 118(18):1837-1847.
26. Landry YD, *et al.* (2006) ATP-binding cassette transporter A1 expression disrupts raft membrane microdomains through its ATPase-related functions. *The Journal of biological chemistry* 281(47):36091-36101.
27. van der Luit AH, *et al.* (2007) A new class of anticancer alkylphospholipids uses lipid rafts as membrane gateways to induce apoptosis in lymphoma cells. *Mol Cancer Ther* 6(8):2337-2345.
28. Weller K, *et al.* (2009) Miltefosine inhibits human mast cell activation and mediator release both in vitro and in vivo. *J Invest Dermatol* 129(2):496-498.
29. Gulshan K, Brubaker G, Wang S, Hazen SL, & Smith JD (2013) Sphingomyelin Depletion Impairs Anionic Phospholipid Inward Translocation and Induces Cholesterol Efflux. *The Journal of biological chemistry*.
30. Robinet P, Wang Z, Hazen SL, & Smith JD (2010) A simple and sensitive enzymatic method for cholesterol quantification in macrophages and foam cells. *Journal of lipid research* 51(11):3364-3369.
31. Michelsen KS, *et al.* (2004) Lack of Toll-like receptor 4 or myeloid differentiation factor 88 reduces atherosclerosis and alters plaque phenotype in mice deficient in apolipoprotein E. *Proceedings of the National Academy of Sciences of the United States of America* 101(29):10679-10684.
32. Ito A, *et al.* (2015) LXRs link metabolism to inflammation through Abca1-dependent regulation of membrane composition and TLR signaling. *eLife* 4:e08009.
33. Dong F, Mo Z, Eid W, Courtney KC, & Zha X (2014) Akt inhibition promotes ABCA1-mediated cholesterol efflux to ApoA-I through suppressing mTORC1. *PloS one* 9(11):e113789.
34. Janoudi A, Shamoun FE, Kalavakunta JK, & Abela GS (2016) Cholesterol crystal induced arterial inflammation and destabilization of atherosclerotic plaque. *European heart journal* 37(25):1959-1967.
35. Juliana C, *et al.* (2012) Non-transcriptional priming and deubiquitination regulate NLRP3 inflammasome activation. *The Journal of biological chemistry* 287(43):36617-36622.
36. Ding J, *et al.* (2016) Pore-forming activity and structural autoinhibition of the gasdermin family. *Nature* 535(7610):111-116.

37. Kayagaki N, *et al.* (2015) Caspase-11 cleaves gasdermin D for non-canonical inflammasome signalling. *Nature* 526(7575):666-671.
38. Westerterp M, *et al.* (2013) Deficiency of ATP-Binding Cassette Transporters A1 and G1 in Macrophages Increases Inflammation and Accelerates Atherosclerosis in Mice. *Circulation research* 112(11):1456-1465.
39. Westerterp M, *et al.* (2017) Cholesterol Accumulation in Dendritic Cells Links the Inflammasome to Acquired Immunity. *Cell metabolism* 25(6):1294-1304 e1296.
40. Heid ME, *et al.* (2013) Mitochondrial reactive oxygen species induces NLRP3-dependent lysosomal damage and inflammasome activation. *Journal of immunology* 191(10):5230-5238.
41. Iyer SS, *et al.* (2013) Mitochondrial cardiolipin is required for Nlrp3 inflammasome activation. *Immunity* 39(2):311-323.
42. Dorlo TP, Balasegaram M, Beijnen JH, & de Vries PJ (2012) Miltefosine: a review of its pharmacology and therapeutic efficacy in the treatment of leishmaniasis. *J Antimicrob Chemother* 67(11):2576-2597.
43. Rios-Marco P, Marco C, Cueto FJ, Carrasco MP, & Jimenez-Lopez JM (2016) Pleiotropic effects of antitumour alkylphospholipids on cholesterol transport and metabolism. *Exp Cell Res* 340(1):81-90.
44. Jimenez-Lopez JM, Rios-Marco P, Marco C, Segovia JL, & Carrasco MP (2010) Alterations in the homeostasis of phospholipids and cholesterol by antitumor alkylphospholipids. *Lipids in health and disease* 9:33.
45. Nandi S, *et al.* (2009) ABCA1-mediated cholesterol efflux generates microparticles in addition to HDL through processes governed by membrane rigidity. *Journal of lipid research* 50(3):456-466.
46. Czech MP (2000) PIP2 and PIP3: complex roles at the cell surface. *Cell* 100(6):603-606.
47. Nitulescu GM, *et al.* (2016) Akt inhibitors in cancer treatment: The long journey from drug discovery to clinical use (Review). *Int J Oncol* 48(3):869-885.
48. Matsui Y, *et al.* (2007) Distinct roles of autophagy in the heart during ischemia and reperfusion: roles of AMP-activated protein kinase and Beclin 1 in mediating autophagy. *Circulation research* 100(6):914-922.
49. van Hout GP, *et al.* (2017) The selective NLRP3-inflammasome inhibitor MCC950 reduces infarct size and preserves cardiac function in a pig model of myocardial infarction. *European heart journal* 38(11):828-836.
50. van der Heijden T, *et al.* (2017) NLRP3 Inflammasome Inhibition by MCC950 Reduces Atherosclerotic Lesion Development in Apolipoprotein E-Deficient Mice-Brief Report. *Arteriosclerosis, thrombosis, and vascular biology* 37(8):1457-1461.
51. Evavold CL, *et al.* (2017) The Pore-Forming Protein Gasdermin D Regulates Interleukin-1 Secretion from Living Macrophages. *Immunity*.
52. Chen J & Chen ZJ (2018) PtdIns4P on dispersed trans-Golgi network mediates NLRP3 inflammasome activation. *Nature*.
53. Zhou R, Tardivel A, Thorens B, Choi I, & Tschopp J (2010) Thioredoxin-interacting protein links oxidative stress to inflammasome activation. *Nature immunology* 11(2):136-140.
54. Lee HM, *et al.* (2013) Upregulated NLRP3 inflammasome activation in patients with type 2 diabetes. *Diabetes* 62(1):194-204.
55. Mridha AR, *et al.* (2017) NLRP3 inflammasome blockade reduces liver inflammation and fibrosis in experimental NASH in mice. *J Hepatol* 66(5):1037-1046.

56. Thomas H (2017) NAFLD: A critical role for the NLRP3 inflammasome in NASH. *Nat Rev Gastroenterol Hepatol* 14(4):197.
57. Vaughan AM & Oram JF (2003) ABCA1 redistributes membrane cholesterol independent of apolipoprotein interactions. *Journal of lipid research* 44(7):1373-1380.
58. Wang S, Gulshan K, Brubaker G, Hazen SL, & Smith JD (2013) ABCA1 mediates unfolding of apolipoprotein AI N terminus on the cell surface before lipidation and release of nascent high-density lipoprotein. *Arteriosclerosis, thrombosis, and vascular biology* 33(6):1197-1205.

## Figure Legends

***Figure 1: A) Miltefosine increases ABCA1 mediated cholesterol efflux.*** RAW264.7 macrophages were labeled with $^3$H-cholesterol and pretreated with or without 300 μM 8Br-cAMP to induce ABCA1 expression. Cholesterol efflux to chase media was performed for 4h at 37ºC in serum-free DMEM without addition of acceptor containing either vehicle, 7.5 μM or 10 μM Miltefosine. Values are % cholesterol efflux mean ± SD, N=5, different letters above the bars show p<0.01 by ANOVA Bonferroni posttest, with separate analyses for ± ABCA1 induction. ***B)*** Western blot analysis of 8Br-cAMP induced RAW264.7 cell total and cell-surface ABCA1 ± 7.5 μM Miltefosine treatment for 4h. ***C)*** Cholesterol efflux (4h at 37ºC) from ABCA1 stably transfected and control HEK293 to serum-free DMEM without addition of acceptor containing either vehicle, 7.5 μM or 10 μM Miltefosine. Values are % cholesterol efflux mean ± SD, N=3-5, different letters above the bars show p<0.01 by ANOVA Bonferroni posttest, with separate analyses for ± ABCA1 induction. ***D)*** Cholesterol efflux (4h at 37ºC) from ABCA1 and ABCA1 (W590S, C1477R) double mutant (DM) stably transfected HEK293 to serum-free DMEM ± 7.5 μM Miltefosine. Values are % cholesterol efflux mean ± SD, N=3, different letters above the bars show p<0.01 by ANOVA Bonferroni posttest.

**Figure 2.** ***Miltefosine disrupts lipid-rafts and inhibits PS flip across plasma membrane.*** **A)** GM1 levels assessed by binding of cholera toxin B (CTB) in RAW macrophages ± 7.5 μM Miltefosine for 16h at 37ºC. ***B)*** Flow cytometry quantification of CTB binding of RAW cells treated ± 7.5 μM Miltefosine for 16h at 37ºC. Values are the mean ± SD of the median fluorescence from 3 independent wells (**, p<0.01 by two-tailed t-test). ***C)*** RAW macrophages were incubated with or without 8Br-cAMP to induce ABCA1 and ± 7.5 μM Miltefosine for 16 hrs. PS exposure was determined Annexin V binding via flow cytometry (different letters above the bars show p<0.01 by ANOVA Bonferroni posttest). ***D)*** Cells were pretreated ± 7.5 μM Miltefosine and incubated with 25 μM NBD-PS at RT for 15 min to assess cellular association of PS. ***E)*** Quantification of NBD-PS translocated inside the cells. RAW macrophages were pretreated ± 7.5 μM Miltefosine and incubated with 25 μM NBD-PS at 37ºC for 15 min in phenol red free DMEM. The cells were subjected to flow cytometry analysis in the presence or absence of sodium dithionite to quench extracellular NBD fluorescence, yielding only intracellular NBD fluorescence (mean ± SD % NBD-PS translocated into the cells; N = 3; ***, p<0.001 by two-tailed t-test).

**Figure. 3.** ***Miltefosine alters plasma membrane PIP2 localization. A***) RAW264.7 cells were stably transfected with 2X-PH-PLCeGFP reporter plasmid and treated ± 7.5 μM Miltefosine for 12h at 37ºC and the localization of the GFP-tagged PIP2 reporter was observed. ***B***) RAW264.7 cells treated as in (A) were fixed, permeabilized, and stained with mouse anti β-actin antibody to observe colocalization of actin with the PIP2 reporter. ***C)*** Live cell imaging of RAW264.7 cells stably transfected with 2X-PH-PLCeGFP reporter plasmid ± 7.5 μM Miltefosine treatment, stained for β-actin with Phalloidin and DAPI counterstained.

**Figure. 4.** ***Miltefosine induces autophagy.*** **A)** RAW264.7 cells or LC3-GFP transfected RAW264.7 cells (lower panel) were treated with ± 7.5 μM Miltefosine, followed by staining with p62 antibody (red, upper panel). LC3-GFP protein (green) localization is shown in the lower panel. ***B, C)*** RAW264.7 cells were treated ± 7.5 μM Miltefosine and autophagic flux was assessed in presence of chloroquine for the last 2 h of incubation. The amount of LC3-II was assessed by western blot and densitometry analysis relative to GAPDH (mean ± SD, N = 3, different letters above the bars represent p<0.001 by ANOVA with Bonferroni posttest). ***D)*** Cellular CE/FC ratio in RAW264.7 cells loaded with 100 μg/ml acetylated low-density lipoprotein (AcLDL) and addition of 2 μg/ml ACAT inhibitor (ACATi) and/or 7.5 μM Miltefosine

as indicated (N=3, mean ± SD; *, p<0.05 vs. control; **, p<0.01 vs. control by ANOVA Bonferroni posttest). ***E)*** Cellular neutral lipids assayed by Nile red staining and flow cytometry ± AcLDL loading, ± 4 hr chase ± 7.5 µM Miltefosine ±2 µg/ml ACATi, as indicated (mean ± SD, N = 4, different letters above the bars represent p<0.0001 by ANOVA with Bonferroni posttest).

***Figure. 5. Miltefosine dampens TLR4 signaling in bone marrow derived macrophages.*** ***A)*** Mouse BMDMs were treated with ± 5 µM Miltefosine for 16h at 37ºC and primed by incubation with ± 1mg/ml LPS at 37ºC for 4hrs, followed by analysis of pro-IL-1β mRNA with β-actin mRNA used as a control (N=6, mean ± SD; different letters above the bars represent p<0.01 by ANOVA with Bonferroni posttest). ***B)*** Mouse BMDMs were treated with ± 5 µM Miltefosine and primed by incubation with ± 1mg/ml LPS followed by western blot analysis for IL1-β with GAPDH used as loading control.

***Figure. 6. Miltefosine inhibits Nlrp3 inflammasome assembly and IL-1β release. A)*** Mouse BMDMs were pretreated with ± 5 µM Miltefosine, primed by incubation with ± 1µg/ml LPS, and induced for NLRP3 inflammasome assembly by incubation with 1 mM ATP for 20 min. Cells were fixed and stained with anti-ASC with DAPI. ***B)*** IL-1β levels in media from cells treated with LPS and ATP ± 5 µM Miltefosine pretreatment. ***C)*** qRT-PCR analysis of NLRP3, caspase 1, and Gasdermin D (GsdmD) mRNAs, relative to β-actin mRNA, from mouse BMDMs ± 5 µM Miltefosine pretreatment, ± LPS treatment (N=6, mean ± SD; different letters represent p<0.05 by ANOVA with Bonferroni posttest). ***D)*** IL-1β released from mouse BMDMs treated with ± 5 µM Miltefosine and primed with 1µg/ml LPS, followed by transfection with 2µg of poly (dA-dT) for 3h to induce the AIM2 inflammasome. ***E)*** Cellular total cholesterol levels were determined in mouse BMDMs treated with ± 5 µM Miltefosine for 16h or 1 mM cyclodextrin for 2h. ***F)*** IL-1β released from mouse BMDMs treated ± 1 mM cyclodextrin for 2h or ± 5 µM Miltefosine for 16h followed by LPS and ATP treatment (mean ± SD, N = 3, different letters above the bars represent p<0.05 by ANOVA with Bonferroni posttest).

***Figure. 7*****. Miltefosine alters mitochondrial homeostasis.** ***A)*** BMDMs pretreated ± 5 µM Miltefosine and treated ± 1µg/ml LPS were stained with MitoSox to observe mitochondrial ROS in live cells. ***B)*** Flow-cytometry analysis showing quantification of MitoSox staining of live BMDMs treated as indicated (mean ± SD, N = 3, different letters above the bars represent p<0.01 by ANOVA with Bonferroni posttest). ***C)*** Live cell flow cytometry of mitochondrial membrane potential detected by TMRM staining of BMDMs pretreated ± 5 µM Miltefosine and treated ± 1µg/ml LPS (mean ± SD, N = 3, different letters above the bars represent p<0.05 by ANOVA with Bonferroni posttest). ***D)*** RAW264.7 cells treated ± 7.5 µM Miltefosine and live cells were stained for mitophagy and lysosomes.

## *Figure 1*

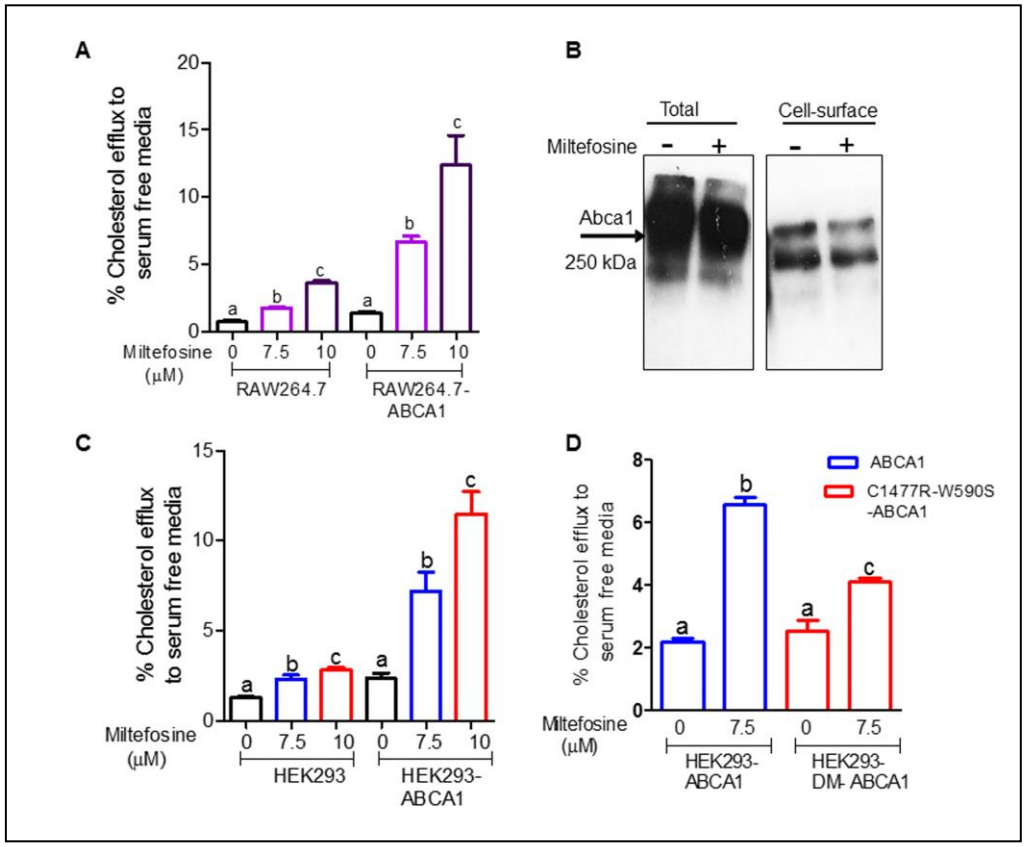
A
% Cholesterol efflux to serum free media
20
15
10
5
0
a
b
c
a
b
c
Miltefosine (μM)
0
7.5
10
0
7.5
10
RAW264.7
RAW264.7-ABCA1
B
Total
Cell-surface
Miltefosine
-
+
-
+
Abca1
250 kDa
C
% Cholesterol efflux to serum free media
15
10
5
0
a
b
c
a
b
c
Miltefosine (μM)
0
7.5
10
0
7.5
10
HEK293
HEK293-ABCA1
D
% Cholesterol efflux to serum free media
8
6
4
2
0
ABCA1
C1477R-W590S -ABCA1
a
b
a
c
Miltefosine (μM)
0
7.5
0
7.5
HEK293-ABCA1
HEK293-DM- ABCA1

## *Figure 2*

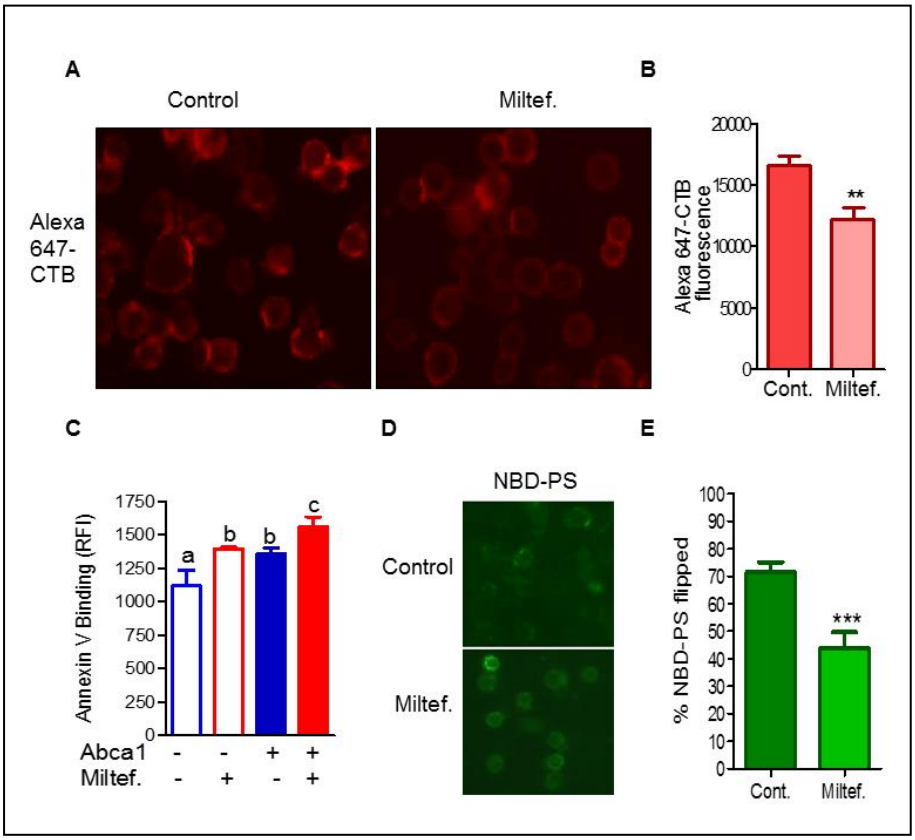
A
Control
Miltef.
Alexa 647-CTB
B
Alexa 647-CTB fluorescence
20000
15000
10000
5000
0
**
Cont.
Miltef.
C
Annexin V Binding (RFI)
1750
1500
1250
1000
750
500
250
0
a
b
b
c
Abca1 - - + +
Miltef. - + - +
D
NBD-PS
Control
Miltef.
E
% NBD-PS flipped
100
90
80
70
60
50
40
30
20
10
0
***
Cont.
Miltef.

## *Figure 3*

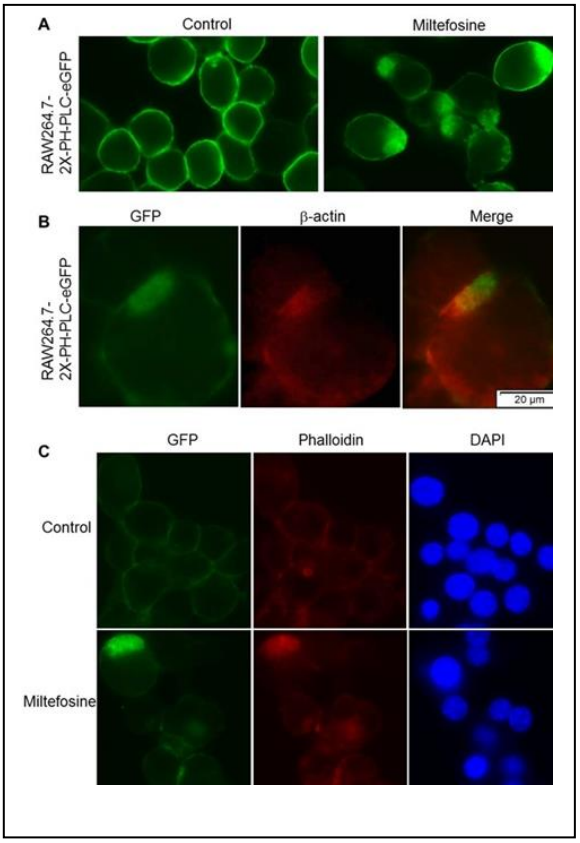
A
Control
Miltefosine
RAW264.7-
2X-PH-PLC-eGFP
B
GFP
β-actin
Merge
RAW264.7-
2X-PH-PLC-eGFP
20 μm
C
GFP
Phalloidin
DAPI
Control
Miltefosine

## *Figure 4*

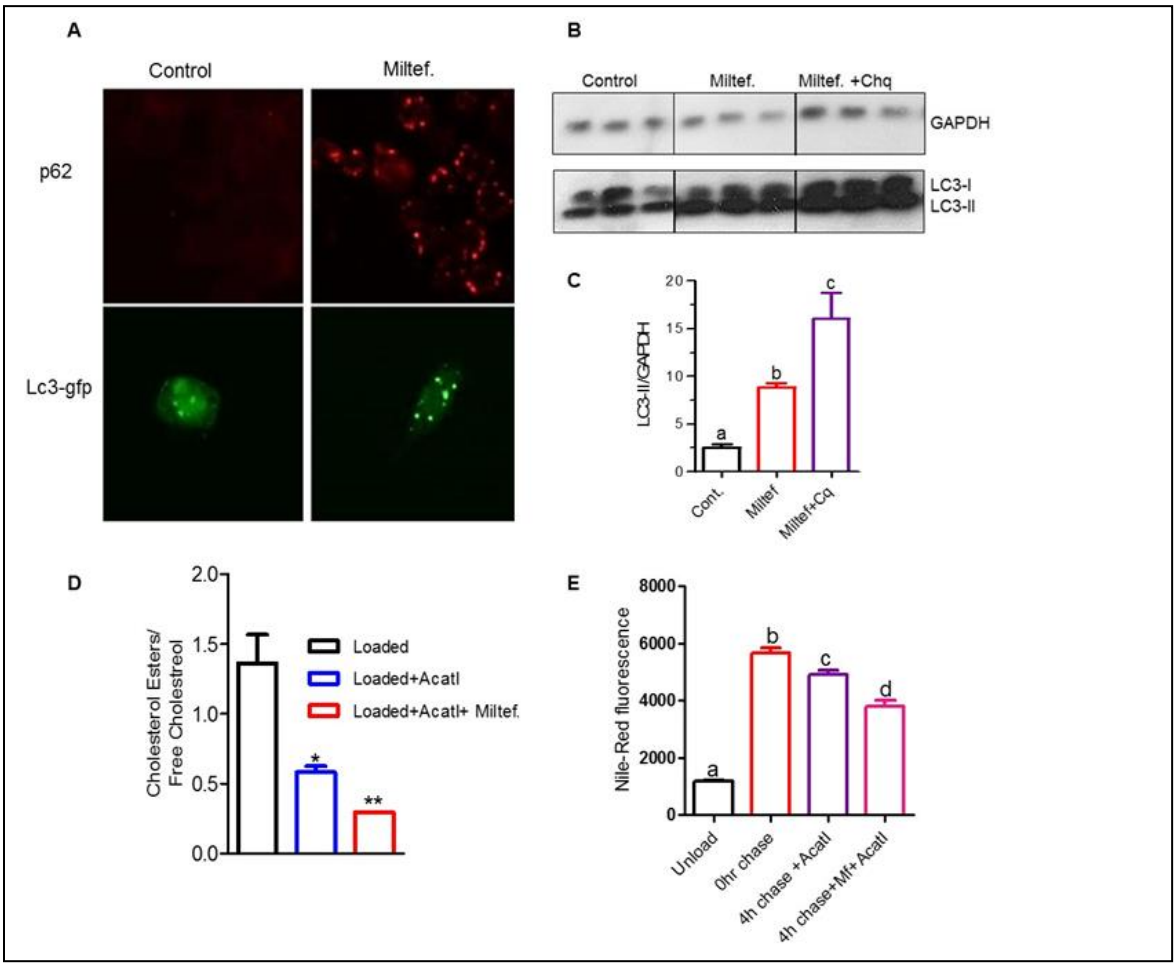
A
Control
Miltef.
p62
Lc3-gfp
B
Control
Miltef.
Miltef. +Chq
GAPDH
LC3-I
LC3-II
C
LC3-II/GAPDH
20
15
10
5
0
a
b
c
Cont.
Miltef
Miltef+Cq
D
Cholesterol Esters/
Free Cholestreol
2.0
1.5
1.0
0.5
0.0
Loaded
Loaded+AcatI
Loaded+AcatI+ Miltef.
*
**
E
Nile-Red fluorescence
8000
6000
4000
2000
0
a
b
c
d
Unload
0hr chase
4h chase +AcatI
4h chase+Mf+AcatI

## *Figure 5*

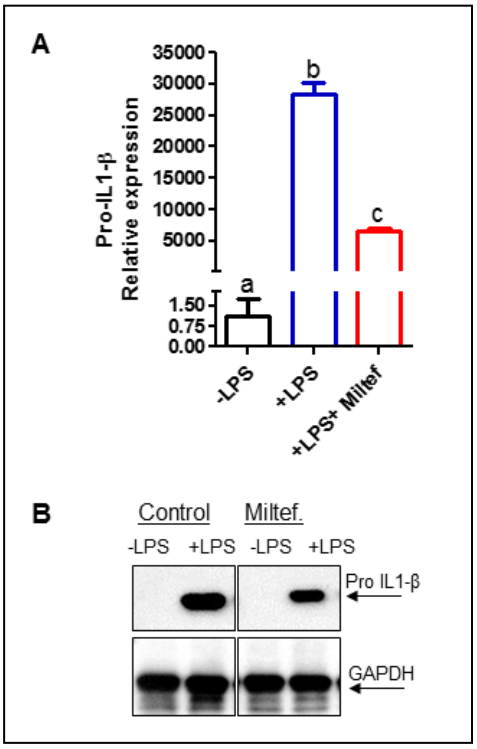
A
Pro-IL1-β
Relative expression
35000
30000
25000
20000
15000
10000
5000
1.50
0.75
0.00
a
b
c
-LPS
+LPS
+LPS+ Miltef
B
Control
Miltef.
-LPS
+LPS
-LPS
+LPS
Pro IL1-β
GAPDH

## *Figure 6*

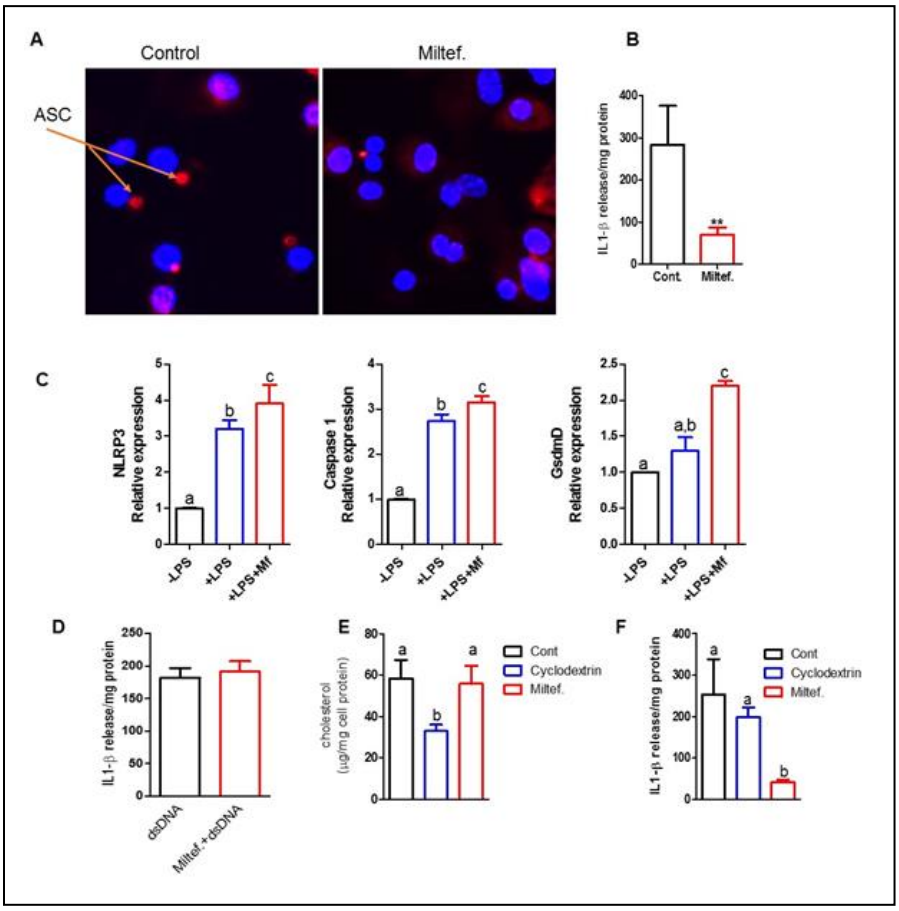
A
Control
Miltef.
ASC
B
IL1-β release/mg protein
400
300
200
100
0
**
Cont.
Miltef.
C
NLRP3
Relative expression
Caspase 1
Relative expression
GsdmD
Relative expression
-LPS
+LPS
+LPS+Mf
a
b
c
a,b
D
IL1-β release/mg protein
250
200
150
100
50
0
dsDNA
Miltef.+dsDNA
E
cholesterol
(µg/mg cell protein)
80
60
40
20
0
Cont
Cyclodextrin
Miltef.
F
IL1-β release/mg protein
400
300
200
100
0
Cont
Cyclodextrin
Miltef.

## *Figure 7*

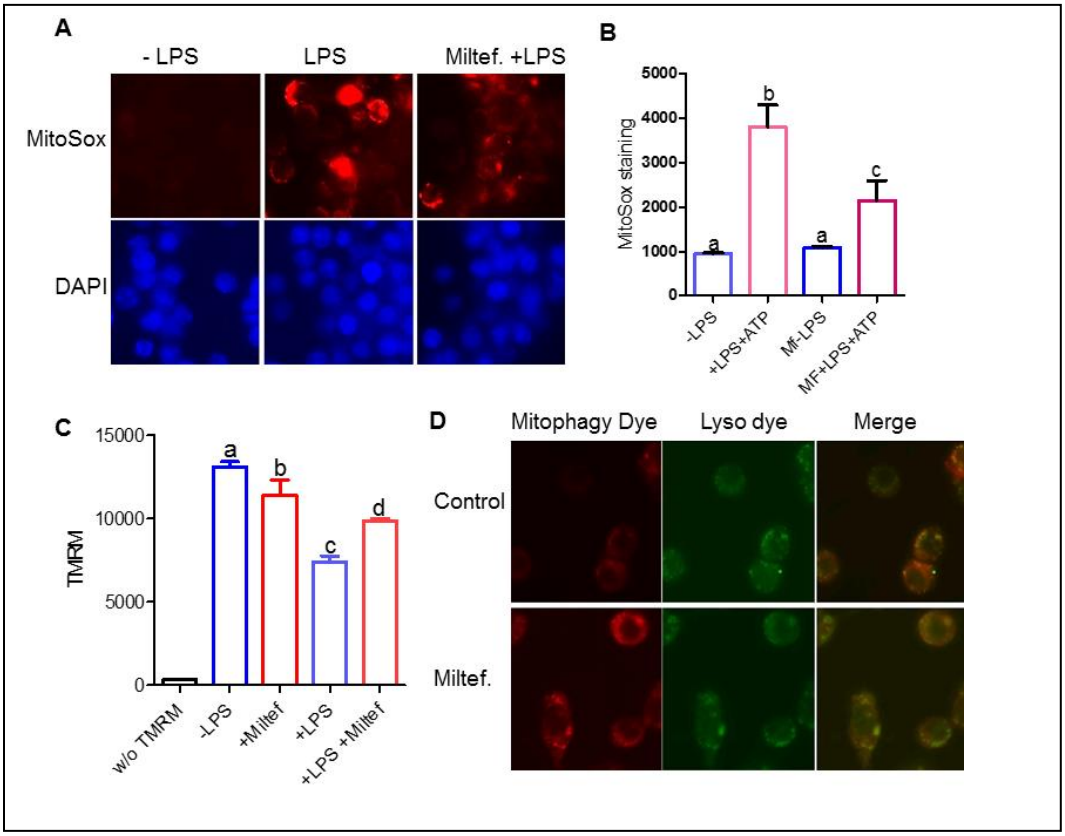
A
- LPS
LPS
Miltef. +LPS
MitoSox
DAPI
B
MitoSox staining
5000
4000
3000
2000
1000
0
a
b
a
c
-LPS
+LPS+ATP
Mf-LPS
MF+LPS+ATP
C
TMRM
15000
10000
5000
0
a
b
c
d
w/o TMRM
-LPS
+Miltef
+LPS
+LPS +Miltef
D
Mitophagy Dye
Lyso dye
Merge
Control
Miltef.

## *SI Materials and Methods*.

***Materials:*** The RAW264.7 cells were from ATCC. Miltefosine and 18:1 NBD-PS were obtained from Avanti polar and methyl-β-cyclodextrin is obtained from Sigma Aldrich. $^{3}$H-cholestreol (NET13900) was obtained from Perkin- Elmer. Antibodies were purchased from various sources (see table below). MitoSox reagent, Image-iT ™ TMRM reagent, and Alexa FluorTM555 Phalloidin were purchased from Invitrogen.

| | | |
|---|---|---|
| NovusBio | ABCA1 | NB400-05 |
| Cell signaling: | GAPDH (14C10) Rabbit mAb | 2118 |
| | NLRP3 (D4D8T) Rabbit mAb | 15101 |
| | NF-κB p65 (C22B4) Rabbit mAb | 4764 |
| | Phospho-AmpKa (The172) (40H9) Rabbit mAb | 2535S |
| | AmpKa Ab | 2532S |
| | Albumin Antibody | #4929 |
| Abclonal | GSDMD | A10164 |
| Invitrogen | Pip4k2a | PA5-31141 |

**Isolation of Bone marrow derived macrophages:** All experiments were performed in accordance with protocols approved by the Cleveland Clinic Institutional Animal Care and Use Committee (ICUC). WT C57BL/6 or C57BL/6 *ApoE*$^{-/-}$ mice were maintained on chow diet and sacrificed at 16 weeks of age. Femurs were collected to isolate and culture bone marrow macrophages using conditioned L-cell media. Mice were euthanized by $CO_2$ inhalation and femoral bones were removed. The marrow was flushed out of the bones into a 50 ml sterile tube using a 10 ml syringe with a 26 gauge needle filled with sterile DMEM. Cells were centrifuged for 5 min at 1,800 rpm at 4°C, followed by two washes with sterile PBS. The cells were resuspended in sterile-filtered BMDM growth media (DMEM with 7.6% fetal bovine serum, 15% L-cell conditioned

media, and 0.76% penicillin/streptomycin mixture) and plated in 10 cm culture dishes and incubated at 37°C for 14 days. Cell media was replaced every 2–3 days for 2 weeks. The cells were routinely visualized under microscope for proliferation and differentiation into confluent BMDMs.

**Isolation of total RNA from BMDM cell pellets and RT-PCR analysis:** Total RNA was isolated from the cell pellets using RNeasy Mini Kit (Qiagen Inc. Valencia, CA). One µg of total RNA was reverse transcribed using the iScript cDNA kit (Biorad). Real-time PCR amplification was performed using TaqMan and gene-specific primers in a StepOnePlus™ real time PCR machine (Applied Biosystems) in triplicate. The relative amount of target mRNA was determined using the cycle threshold (Ct) method by normalizing target mRNA Ct values to that of β-actin. The Fold induction ratios were calculated relative to control sample for each group using the formula $2^{-\Delta\Delta Ct}$.

The reagents were obtained from Qiagen, Biorad, and ThermoFisher (see table below).

| | | |
|---|---|---|
| Qiagen | RNEasy MiniKit | 74104 |
| Qiagen | Rnase-free Dnase set | 79254 |
| Biorad | iScript cDNA kit | 170-8891 |
| ThermoFisher | 2x TaqMan | 4304437 |
| ThermoFisher | NIrp3 | Mm00840904 |
| | Casp1 | Mm00438023 |
| | iL1B | Mm00434228 |
| | Gsdmd | Mm00509958 |
| | Actb | Mm02619580 |

**Cholesterol efflux assay**: The cholesterol efflux assays were performed in HEK293-Abca1-GFP cells, BHK cells, or RAW 264.7 murine macrophages. The cells were plated in 24-well plates at a density of 300-400,000 cells per well. The cells were labeled with $^{3}H$ cholesterol in 1% FBS in DMEM for 24h. The labeled cells were induced for ABCA1 expression for 16h with 0.3 mM 8Br-cAMP (for RAW264.7 cells) or with 10nM

Mifepristone (for BHK cells). Inducers were included in the media during subsequent assays. ABCA1 expression was confirmed by western blot using the AC10 antibody. The cells were washed with serum free media and chased for indicated time period in serum-free DMEM in the presence or absence of indicated treatments. The radioactivity in the chase media was determined after brief centrifugation to pellet any residual debris. Radioactivity in the cells was determined by extraction in hexane:isopropanol (3:2) with the solvent evaporated in a scintillation vial prior to counting. The percent cholesterol efflux was calculated as 100 × (medium dpm) / (medium dpm + cell dpm).

**Lipid-Raft quantification**: The lipid-raft were visualized under fluorescent microscope and quantified using flow-cytometry assay. RAW cells were treated with 7.5 µg/ml Miltefosine at 37ºC for 16h. For imaging, cells were treated with 1 µg/ml Alexa647-CT-B labeled cells and images were captured using epifluorescent microscopy. For quantification, the cells were washed twice with PBS and gently scraped in 1.5 ml PBS. The Alexa647-CT-B (1µl of 1.5 mg/ml stock in PBS was added to 1.5 ml cells) was added at final concentration of 1 µg/ml to cells in 5 ml polystyrene round-bottom tubes (12 X 75 mm). The samples were subjected to Flow analysis with BD Biosciences LSRII cytometer using laser (Alexa 647 (Red) Ex: 639, Em: 650-670, Filter 660/20) and data was analyzed by Flowjo software.

**Cell-surface PS and NBD-PS translocation:** To measure cell surface PS, cells were cultured in 6 well plates in growth media, washed twice with PBS, and were resuspended in 500 µl Annexin V binding buffer plus 1 µl of Annexin V-Cy5 (Biovision). The samples were incubated at room temperature for 5 minutes in the dark. Flow

cytometry analysis was performed using a BD Biosciences LSRFortessa cytometer using a 639 nm excitation laser and emission at 650-670 nm; and, data was analyzed using Flowjo software. To measure the inward translocation of various NBD labeled PS, RAW cells were incubated with phenol-red free DMEM containing 25 μM NBD-PS for 15 min at RT. The media was then replaced with PBS. The cells were gently scraped and were subjected to flow cytometry analysis first without sodium dithionite to calculate total NBD fluorescence, and then 5 min after the addition of 30 μl of a freshly prepared 1M sodium dithionite solution to determine the fraction of the signal resistant to quenching (translocated signal). Flow cytometry analysis was performed as above using a 488 nm laser for excitation and emission at 505-525 nm.

**Western blotting:** RAW264.7 cells or BMDMs were grown treated as indicated. The PBS-washed cell pellet was lysed in NP40 lysis or MPER lysis buffer. After discarding the nuclear pellet, the protein concentration was determined using the BCA protein assay (Pierce). 10-50 μg of cell protein samples were resolved on Novex 4-20% Tris-Glycine Gels (Invitrogen) and transferred onto polyvinylidene fluoride membranes (Invitrogen). Blots were incubated sequentially with 1:1000 rabbit polyclonal antibody raised against Nlrp3 (cell signaling), or 1:5000 rabbit polyclonal antibody raised against P-AMPK (cell signaling), or 1:1000 rabbit polyclonal antibody raised against IL1-b (cell signaling), 1:1000 rabbit polyclonal antibody raised against Gasdermin D, 1:1000 rabbit polyclonal antibody raised against ASC1. The signal was detected with an enhanced chemiluminescent substrate (Pierce). For LC3 western blot, RAW264.7 cells were incubated with or without 7.5 μM Miltefosine for 16 h, indicated wells received 30 μM chloroquine during the last 2 h of incubation. Blots were sequentially incubated with

1:1,000 rabbit polyclonal antibody raised against LC3B and 1:10,000 horseradish peroxidase-conjugated goat anti-rabbit as described above. GAPDH was used as a loading control.

**Total and cell surface ABCA1 levels:** RAW 267.4 cells were cultured in DMEM with 10% FBS and were treated with 300 μM 8Br-cAMP to induce ABCA1 for 16 hr. Cells were incubated with incubated with or without 7.5μM Miltefosine for 4h. The cells were then incubated for 30 minutes on ice with phosphate-buffered saline (PBS) containing 1 mg/mL sulfo-NHS-biotin (Pierce). The PBS-washed cell pellet was lysed in 200 μl of lysis buffer (150 mM sodium chloride, 5 mM EDTA, 50 mM Tris-phosphate pH 8.0, 1% NP40, and 10% protease inhibitor). Cell-surface ABCA1 was determined by purifying biotinylated proteins by overnight incubation of 250 ug of cell protein with 75 uL of UltraLink Plus Immobilized Streptavidin gel (Pierce) at 4°C. The beads were spun down, washed, and resuspended by boiling in 100 μl 1x NuPage LDS Sample buffer (Invitrogen) and 20 μg of total protein were run on NuPAGE 3-8% Tris-Acetate gels (Invitrogen) and transferred onto polyvinylidene fluoride membranes (Invitrogen). Blots were incubated sequentially with 1:500 mouse monoclonal antibody raised against ABCA1 (AC10) and 1:15 000 horseradish peroxidase-conjugated goat anti-mouse secondary antibody (Biorad). The signal was detected with an enhanced chemiluminescent substrate (Pierce).

## Supplementary Figure Legends

***Figure S1: Miltefosine increased ABCA1 mediated cholesterol efflux. A)*** The LDH release assay showing % LDH release in RAW264.7 macrophages as compared to control cells (mean ± SD, N=3, different letters above the bars show $p<0.001$ by ANOVA Bonferroni posttest, all columns compared to control column). ***B)*** The LDH

release assay showing % LDH release in BMDMs as compared to control cells(mean ± SD, N=3, different letters above the bars show p<0.001 by ANOVA Bonferroni posttest, all columns compared to control column). ***C)*** BHK cells were labeled with $^{3}$H-cholesterol and pretreated with or without Mifepristone to induce ABCA1 expression. Cholesterol efflux to chase media was performed for 4h at 37ºC in serum-free DMEM without addition of acceptor containing either vehicle, 7.5 μM or 10 μM Miltefosine. Values are % cholesterol efflux, mean ± SD, N=5, different letters above the bars show p<0.01 by ANOVA Bonferroni posttest, with separate analyses for ± ABCA1 induction. ***D)*** The WT ABCA1-GFP and double mutant ABCA1-GFP isoform expression measured by flow cytometry analysis (Values are GFP intensity, mean ± SD, N=4, different letters above the bars show p<0.0001 by two-tailed t-test.

***Figure S2: Miltefosine increased microparticle generation.*** RAW cells were treated with ± 7.5 µM Miltefosine for 4h at 37ºC. The media was collected and cleared of cell debris by centrifugation at 5K rpm for 5 min. The supernatant was spun down at 15K for 30 min. The pellet was suspended in sterile PBS (filtered with 0.22 µM filter) and microparticle were detected using Zetaview particle analyzer. Values are number of microparticles per ml, mean ± SD, N=3, different letters above the bars show p<0.001 by t-test.

***Figure S3: Miltefosine decreased lipid droplets.*** RAW cells were loaded with 100μg/ml AcLDL for 24h, followed by 4 hr chase ± 7.5 µM Miltefosine for 4h at 37ºC. The cells were then stained with Nile-red and counterstained with DAPI and imaged using fluorescent microscope.

***Figure S4: Miltefosine induced AMPK phosphorylation.*** RAW cells were treated ± 7.5 µM Miltefosine for 4h at 37ºC. The cells extracts were prepared in MPER lysis buffer containing phosSTOP (Roche). Western blot analysis was carried out using anti-Phosho-AMPK and AMPK antibodies.

***Figure S5: Miltefosine inhibited Nlrp3 inflammasome assembly.*** Full image of cropped section shown in ***Figure 6A***. Asc specks and DAPI staining in control BMDMs.

***Figure S6: Miltefosine inhibited Nlrp3 inflammasome assembly.*** Full image of cropped section shown in ***Figure 6A***. Asc specks and DAPI staining in Miltefosine treated BMDMs.

***Figure S7: Miltefosine did not alter the protein levels of Nlrp3 inflammasome complex.*** Mouse BMDMs were treated with ± 5 µM Miltefosine for 16h at 37ºC. The cells were primed by incubation with ± 1mg/ml LPS at 37ºC for 4hrs, followed by cell extract preparation and western blot analysis using NLRP3 antibody (***A***), ASC (***B***), Caspase 1 (***C***) and Gasdermin D (***D***). GAPDH was used as loading control.

***Figure S8: Miltefosine inhibited Nlrp3 inflammasome assembly.*** Asc specks and DAPI staining in cyclodextrin treated BMDMs.

***Figure S9: Miltefosine altered mitochondrial homeostasis.*** TMRM staining of mouse BMDMs pretreated ± 5 µM Miltefosine and treated ± 1μg/ml LPS.

***Figure S10: Miltefosine altered mitochondrial homeostasis.*** Mouse BMDMs pretreated ± 5 µM Miltefosine were stained with mitophagy dye (Mitophagy detection kit MD01, Dojindo Molecular Technologies, Inc.)

***Figure S1***

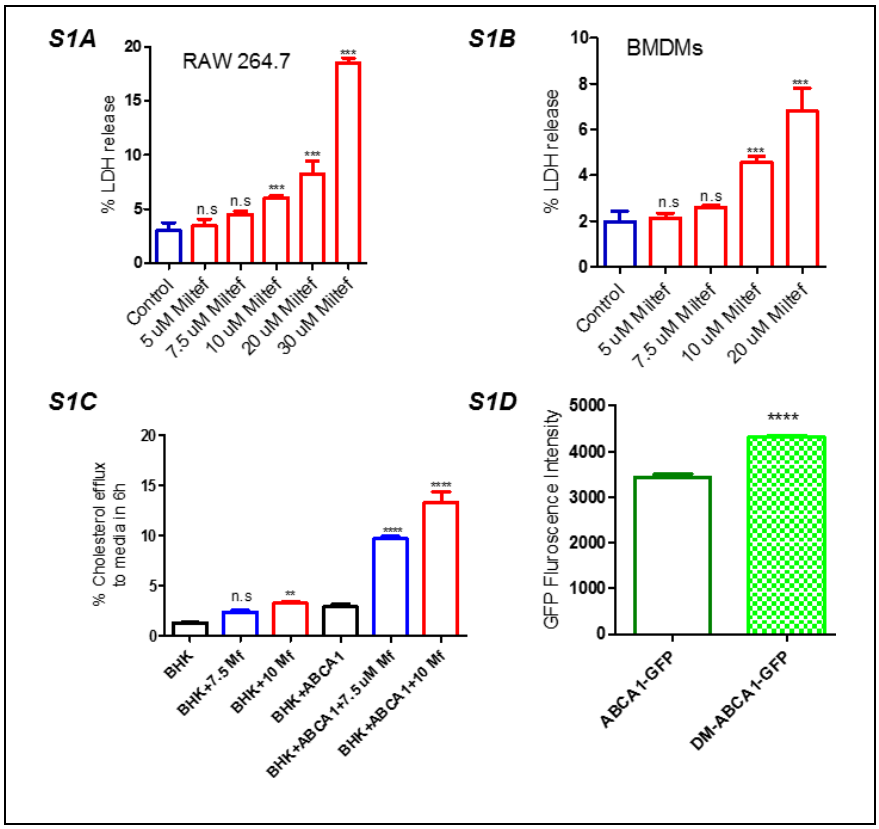
S1A
RAW 264.7
% LDH release
20
15
10
5
0
n.s
n.s
***
***
***
Control
5 uM Miltef
7.5 uM Miltef
10 uM Miltef
20 uM Miltef
30 uM Miltef
S1B
BMDMs
% LDH release
10
8
6
4
2
0
n.s
n.s
***
***
Control
5 uM Miltef
7.5 uM Miltef
10 uM Miltef
20 uM Miltef
S1C
% Cholesterol efflux to media in 6h
20
15
10
5
0
n.s
**
****
****
BHK
BHK+7.5 Mf
BHK+10 Mf
BHK+ABCA1
BHK+ABCA1+7.5 uM Mf
BHK+ABCA1+10 Mf
S1D
GFP Fluroscence Intensity
5000
4000
3000
2000
1000
0
****
ABCA1-GFP
DM-ABCA1-GFP

***Figure S2***

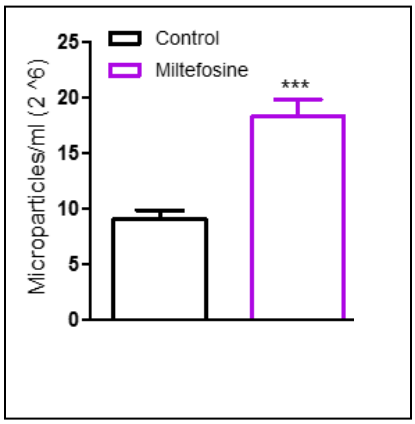

***Figure S3, S4***

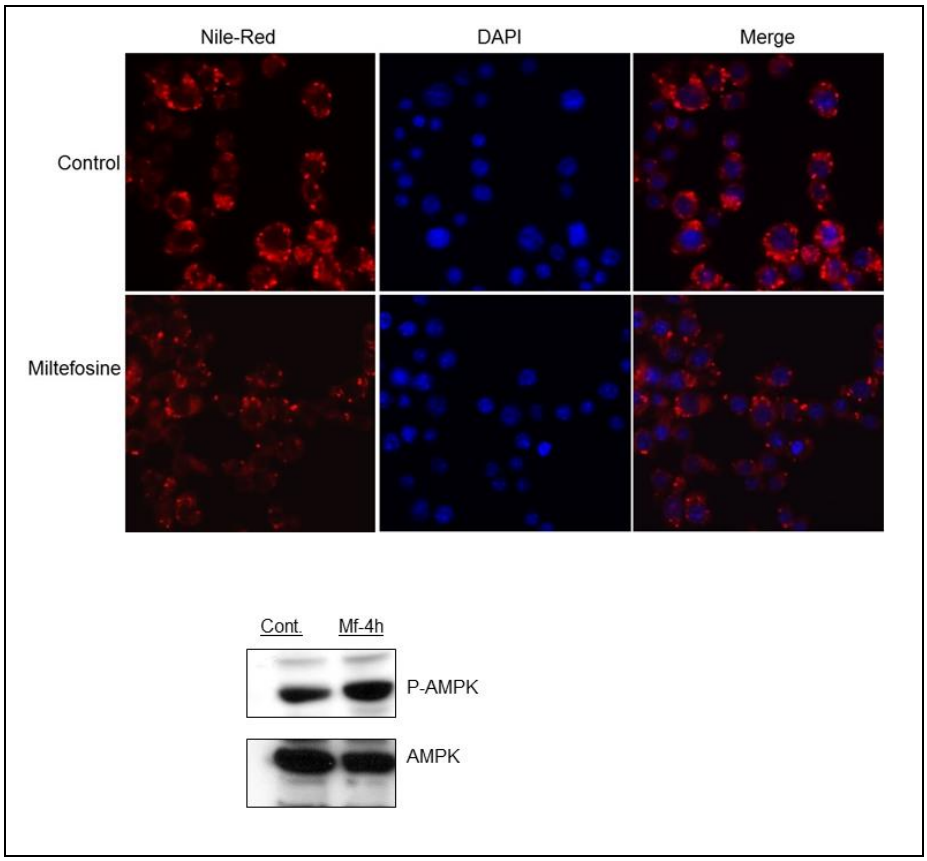
Nile-Red
DAPI
Merge
Control
Miltefosine
Cont.
Mf-4h
P-AMPK
AMPK

*Fig. S5*

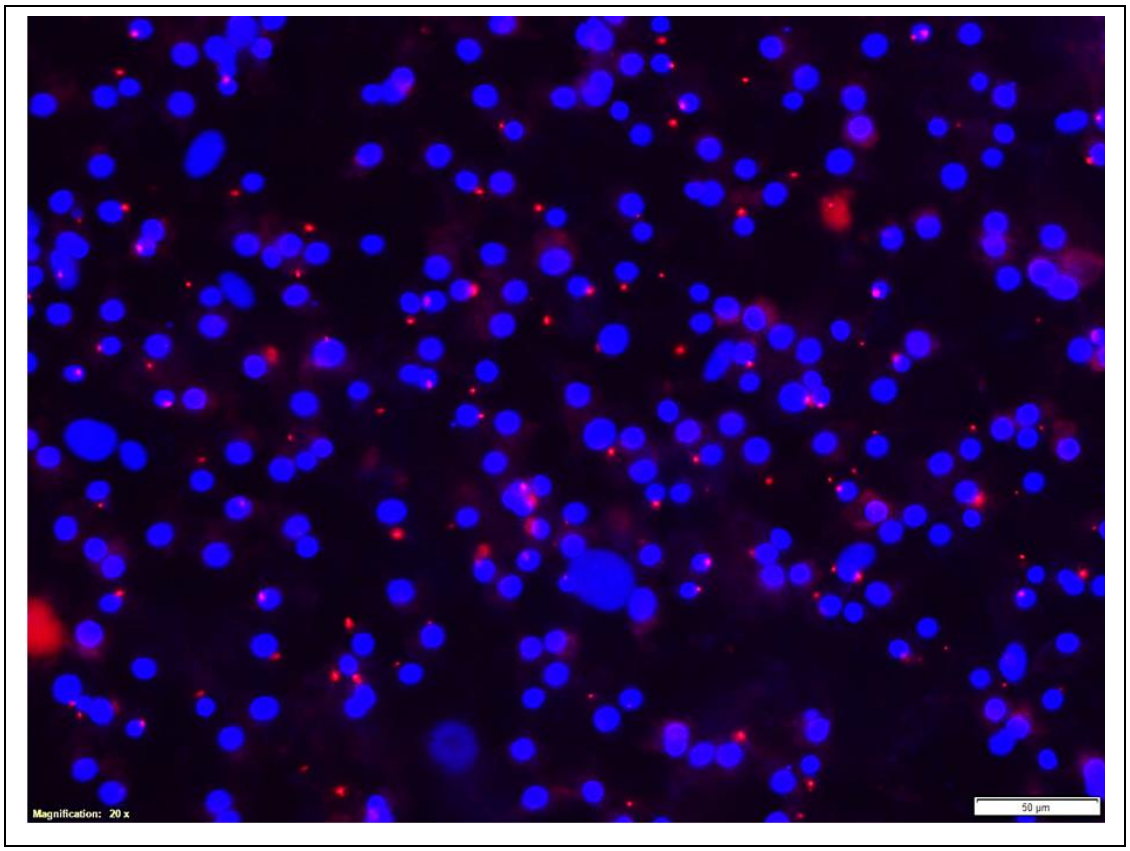

*Fig. S6*

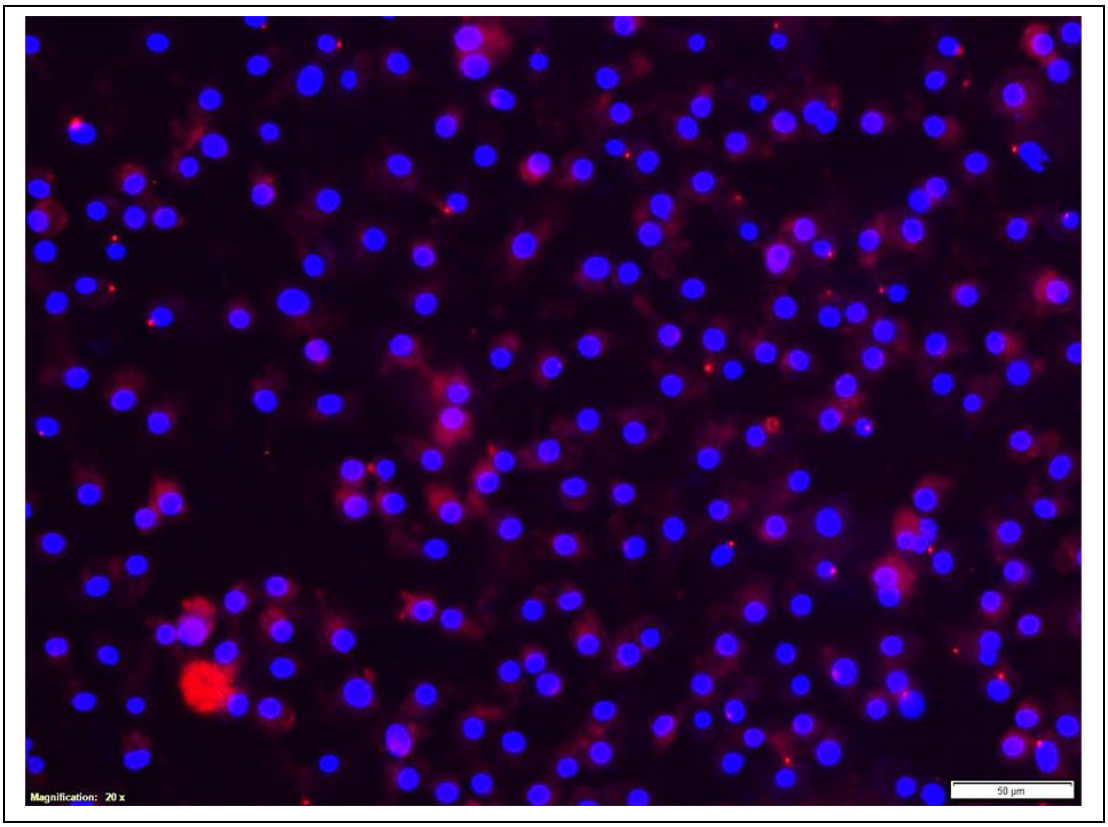

*Fig. S7*

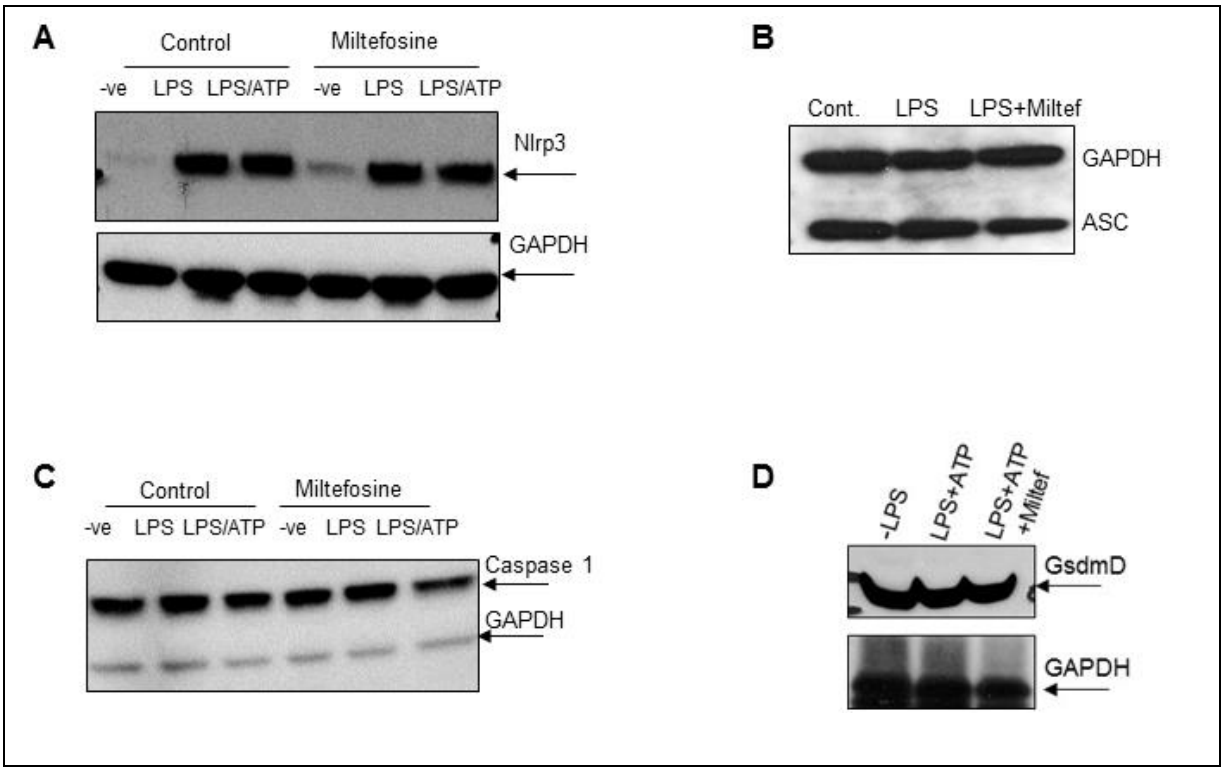
A
Control
Miltefosine
-ve
LPS
LPS/ATP
-ve
LPS
LPS/ATP
Nlrp3
GAPDH
B
Cont.
LPS
LPS+Miltef
GAPDH
ASC
C
Control
Miltefosine
-ve
LPS
LPS/ATP
-ve
LPS
LPS/ATP
Caspase 1
GAPDH
D
-LPS
LPS+ATP
LPS+ATP +Miltef
GsdmD
GAPDH

*Fig. S8*

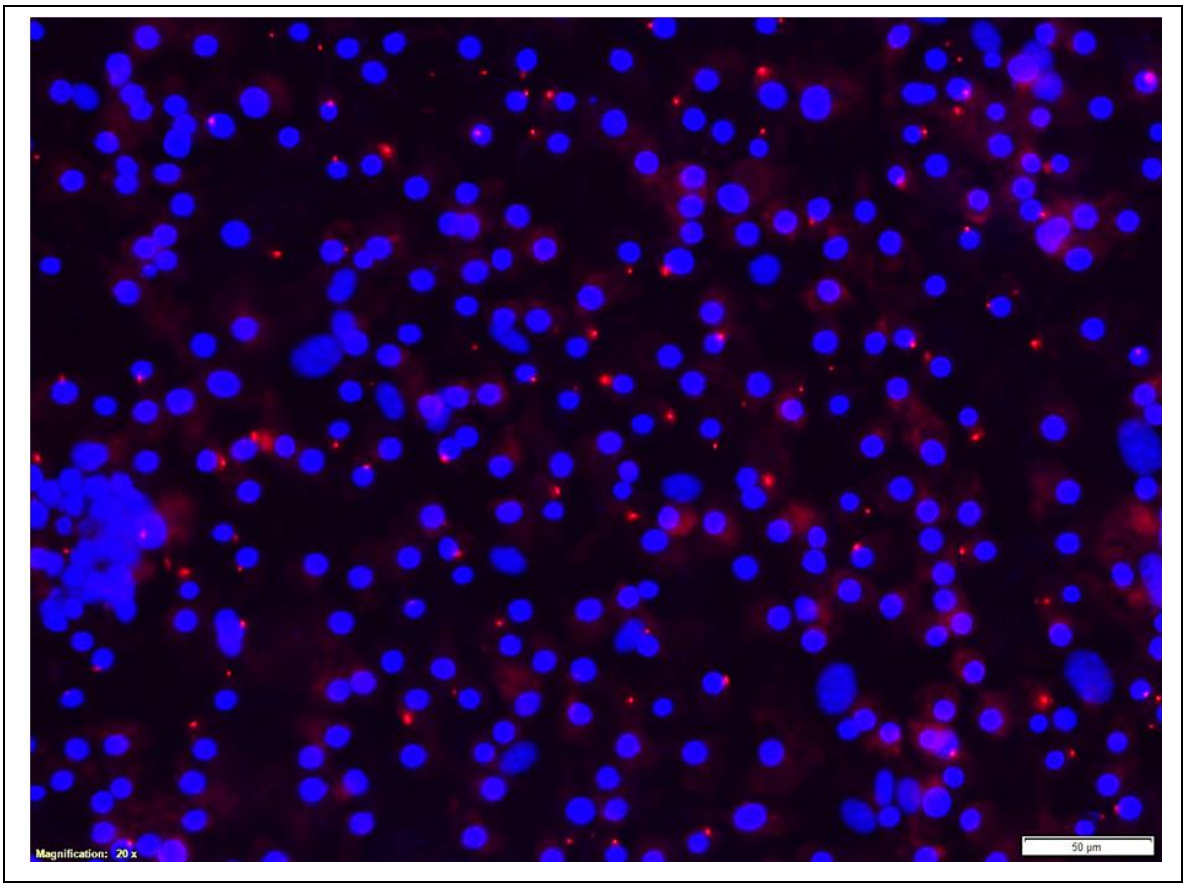

*Fig. S9*

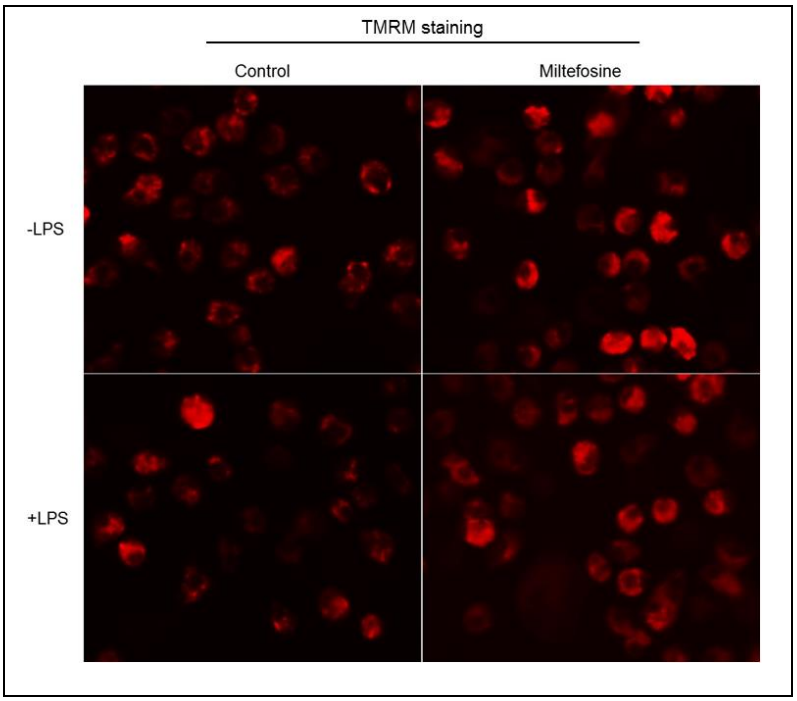
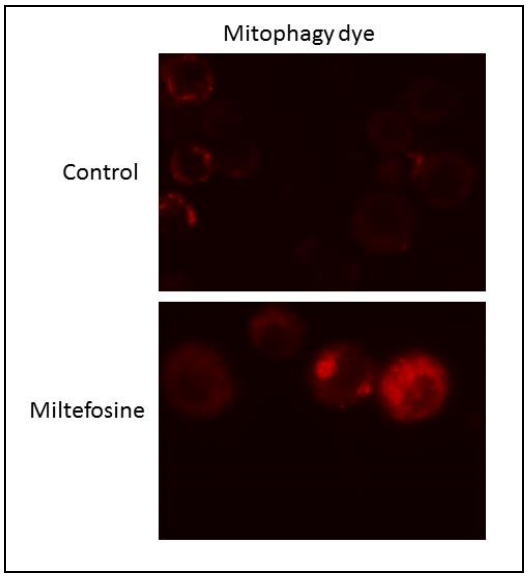
***Fig. S10***